Non-invasive blood pressure monitoring with in-ear infrasonic hemodynography for preventative cardiovascular care

Check for updates

Robert Ciesielski[1], Christine S. Wong[2], Jal Panchal[1], Jacek Grela[1], Christina Dimalanta[2], Alison Walton[2], Hayley Engstrom[2], Martin D. Ring[1], Jacob Abraham[3], Curtiss Stinis[2], Steven Romero[2] & Anna Barnacka[1] ✉

Infrasonic Hemodynography (IH) captures low-frequency vibrations detected by in-ear microphones, offering a new approach to blood pressure monitoring. We report a strong correlation (r = 0.95) between IH waveforms and aortic blood pressure measurements obtained through cardiac catheterization (CC). Temporal analysis confirms the aortic origin of IH signals, with minimal differences in aortic valve opening timings between IH and CC (1.6 ± 12.1 ms), rejecting the hypothesis of peripheral origins. We test an approach to predict systolic (SBP) and diastolic (DBP) blood pressure from waveform morphology. The standard deviations of the differences between predicted and reference BP values averaged across 12 subjects is 4.1 mmHg (SBP) and 2.4 mmHg (DBP) for CC, and 5.8 mmHg (SBP) and 3.7 mmHg (DBP) for IH. These results demonstrate that BP information is encoded in the waveform shape dynamic. By capturing precise cardiovascular signals non-invasively, IH could enable earlier interventions and more personalized treatments.

Blood pressure monitoring is essential for managing hypertension, reducing post-hospital readmissions, and evaluating the hemodynamic effects and cardiac safety of drugs during clinical trials[1–6]. Although diagnosing hypertension is relatively simple, and the condition can be effectively treated with affordable medications, there are substantial gaps in both diagnosis and treatment. Approximately 580 million individuals with hypertension, among them 41% of women and 51% of men population, remain unaware of their condition due to a lack of diagnosis[7]. Digitally connected blood pressure monitors provide a viable alternative to traditional office-based monitoring. While several cuffless blood pressure monitors are currently under development, they require additional validation before they can be widely adopted for clinical use[8–11]. Several cuffless, continuous non-invasive blood pressure (NIBP) monitoring technologies have emerged in recent years, including photoplethysmography (PPG)-based approaches such as the Hilo (previously Aktiia) bracelet, pulse transit time (PTT)-based devices like those developed by Biobeat, and continuous finger cuff technologies such as the CNAP system. As the adoption of wearable devices continues to rise, there is a growing need and opportunity to implement a multifaceted approach to integrate these technologies into both clinical practice and consumer routines. This approach is essential to effectively manage the increasing global population with hypertension.

In this context, Infrasonic Hemodynography (IH) emerges as a promising path. IH is a novel, non-invasive technology that measures in-ear

acoustic pressure using microphones leveraging existing existing technologies, particularly those with noise cancellation features that already have microphone facing ear canal built in. These earbuds can simultaneously be used for biosignal recording. IH focuses on detecting low-frequency vibrations (<20 Hz) generated by vital organs, especially the cardiovascular system, as acoustic waveforms. By capturing sound signals traveling within arteries, fluids, bones, and muscles to the ear canal, IH enables the measurement of an individual's unique "audiome." The low-frequency nature of these biosignals, falling below the threshold of human hearing, allows biosignal monitoring without disrupting the primary function of the earbuds, such as music playback or calls[12].

Previous research on IH has demonstrated a high correlation (r = 0.99) between IH and electrocardiogram (ECG) measurements for interbeat intervals and heart rate in stationary conditions, as well as IH's capability to monitor physiological changes induced by breathing without compromising accuracy, even during music playback[12]. Furthermore, algorithms based on IH data have been shown to distinguish between atrial fibrillation and sinus rhythm with performance comparable to ECG[12]. IH technology also measures interbeat intervals for various cardiac rhythms and heart rates with the same accuracy as ECG while providing additional hemodynamic insights not accessible through ECG[13]. In a first in-person study, IH demonstrated high accuracy in capturing cardiovascular time intervals and performance measures compared to echocardiography and invasive cardiac

[1]MindMics, Inc, Cambridge, MA, USA. [2]Division of Cardiology, Scripps Clinic, La Jolla, CA, USA. [3]Center for Cardiovascular Analytics, Research and Data Science (CARDS), Providence Heart Institute, Providence Research Network, Portland, OR, USA. ✉e-mail: anna.barnacka@mindmics.com

catheterization hemodynamic waveforms[14]. For instance, IH has been shown to synchronize with the Wiggers diagram in severe aortic stenosis, detecting murmurs consistent with the condition before transcatheter aortic valve replacement (TAVR) and showing resolution of these murmurs after TAVR[15]. IH's ability to identify such changes non-invasively underscores its potential as a novel method for early detection of aortic stenosis and other cardiovascular conditions[16].

Although previous studies have highlighted IH's potential for cardiac rhythm analysis and hemodynamic assessment, there has been limited exploration of its application for NIBP estimation. The methodology presented in this work introduces a novel approach to continuous, cuffless blood pressure monitoring based on waveform features extracted from IH signals recorded in the ear canal. Unlike existing systems, our approach leverages consumer-grade wireless earbuds, incorporates multimodal alignment with invasive gold-standard data, and applies machine learning models trained on pressure waveforms. This positions our work as the first to validate IH-based NIBP estimation against catheterization data. By offering non-invasive, and highly accurate cardiac signal measurements via earbuds, IH represents a significant advancement in hemodynamic monitoring. IH captures infrasonic waves that directly correlate with central blood pressure waveforms, providing a promising pathway to deliver accurate and user-friendly blood pressure monitoring.

Understanding the cardiac cycle is essential for interpreting the data and building reliable predictive algorithms. The cardiac cycle consists of a series of pressure changes that lead to the movement of blood through the chambers of the heart, divided into two main phases: diastole and systole.

Diastole encompasses ventricular relaxation and filling, including rapid inflow, diastasis, atrial systole, and isovolumetric relaxation. It begins with the closing of the aortic and pulmonic valves and ends with the closing of the mitral and tricuspid valves[17,18]. On the ECG, diastole is often timed between the T wave and the subsequent R wave[19]. Early diastolic filling starts with the opening of the mitral valve, allowing blood to flow from the atria into the ventricles[20]. During the late filling phase, atrial contraction pushes additional blood into the ventricles. Flow continues until there is equalization of pressure across the atrioventricular valves, leading to their closure and marking the end of diastole. Closure of the mitral and tricuspid valves constitutes the first heart sound, denoted as S1[21].

Systole represents ventricular contraction, during which blood is ejected across the aortic valve to the rest of the body. It begins with the closure of the mitral and tricuspid valves (S1) and concludes with the closure of the aortic and pulmonic valves (S2)[22,23]. Systole is subdivided into isovolumetric contraction and ventricular ejection. Isovolumetric contraction marks the beginning of systole and is the period between the closure of the mitral valve and the opening of the aortic valve. During this time, intrachamber pressure increases without a change in volume. When the pressure within the ventricle exceeds systemic pressure, the aortic valve opens, leading to rapid ventricular ejection. As blood exits the ventricle, the pressure within the chamber drops below systemic pressure, causing the aortic valve to close. The simultaneous closure of the aortic and pulmonic valves comprises the second heart sound, S2[24].

IH signals can be considered the output of the cardiovascular system—a mechanical system—where the input is the electrical activity initiating the cardiac cycle, as traced by the ECG. The IH signals provide a detailed picture of valve function and hemodynamic responses, complementing ECG signals that contain the "trigger" information initiating heart contraction. By providing an accurate and non-invasive depiction of the central cardiovascular system's response, IH technology paves the way for future possibilities to diagnose cardiovascular abnormalities.

In this study, we investigate the correlation between IH waveforms and gold-standard techniques such as ECG, echocardiograms, and invasive aortic blood pressure measurements obtained via cardiac catheterization (CC), using data collected at Scripps Health from 18 subjects who underwent CC for evaluation of the coronary artery disease. The results are illustrated in the form of Wiggers diagrams, providing a visual comparison of cardiovascular waveforms. Moreover, using a subsample of 12 Scripps

subjects with at least 1.5 min of simultaneous CC and IH signals, we develop a machine learning model to predict systolic (SBP) and diastolic (DBP) blood pressure from individual waveforms. Unlike many existing cuffless blood pressure monitoring methods that rely on peripheral signals and require frequent calibration due to physiological variations (e.g., vasoconstriction, body position, hydration, or sympathetic tone)[25–29], the approach presented here is based on IH waveforms that closely correlate with central aortic pressure. To improve robustness, we normalize each cardiac cycle and extract features based on waveform morphology rather than amplitude. This enables our models to capture pressure-related dynamics while eliminating the impact of peripheral physiological changes, reducing the need for frequent recalibration, addressing a common limitation in existing non-invasive blood pressure monitoring devices. Our results demonstrate that waveform shape alone can provide sufficient accuracy for blood pressure prediction.

Following the presentation of results, we discuss the broader implications of IH technology, highlighting its potential for continuous, non-invasive, and contextual blood pressure monitoring. This innovation could drive the future of predictive and proactive healthcare by combining advancements in artificial intelligence with reliable real-time data from in-ear devices. We also address the limitations of the current study, primarily the sample size and the need for further validation in larger, more diverse populations. In the Methods section, we provide a detailed overview of IH technology, the data sample and collection procedures, and the method used to predict SBP and DBP. This article outlines the technical aspects supporting our findings and sets the foundation for future studies aimed at refining and scaling the application of IH technology in clinical and everyday settings.

Results
Wiggers diagrams
In a clinical study conducted at Scripps Health (ClinicalTrials.gov ID: NCT04636892), we analyzed data from 18 study subjects to assess the capabilities of in-ear IH technology in non-invasively representing the cardiac cycle. In-ear acoustic pressure was measured using IH signals recorded simultaneously with data from standard cardiac monitoring devices, including Doppler echocardiography (ECHO) imaging of flow through the left ventricular outflow tract (LVOT) at rest, invasive cardiac catheterization (CC) with a catheter in the aorta, and 12-lead ECG recordings.

Figures 1 and 2 present Wiggers diagrams[30,31] derived from data collected from two exemplary study subjects who wore the IH earbuds during CC for evaluation of coronary artery disease (CAD). Wiggers diagrams for the remaining study subjects are shown in Supplementary Figs. 1 and 2, to illustrate the diversity of measured waveform morphologies. The data, sampled at 1000 Hz, were aggregated into a multimodal time-series dataset. Each plot in Figs. 1 and 2 displays, from top to bottom: (a) Doppler echocardiography imaging of flow through the LVOT at rest, (b) aortic catheterization waveforms, (c) IH waveforms corrected for instrumental effects and converted to in-ear acoustic pressure units, (d) IH waveforms filtered to frequencies above 20 Hz to indicate the presence of S1 and S2 heart sounds, (e) 12-lead (ECG tracings. The distributions represent signals from 15 consecutive cardiac cycles stacked together to obtain average waveforms.

Figures 1 and 2 also include lines marking key cardiac functions and additional details that demonstrate alignment and indicate the timing of specific events and intervals during cardiac cycles. The presented Wiggers diagrams illustrate key features of the cardiac cycle and demonstrate the capabilities of in-ear IH technology to non-invasively capture and represent hemodynamic events. The data show that features of the aortic CC waveforms are also present in the IH waveforms. In both aortic pressure and IH waveforms, we observe distinct morphological features characteristic of the aortic pulse pressure waveform. The systolic upstroke in the IH waveform corresponds to the rapid pressure rise in the aortic waveform, culminating in the systolic peak—representing the maximal pressure during ventricular ejection. During this phase, the anacrotic notch, a subtle inflection
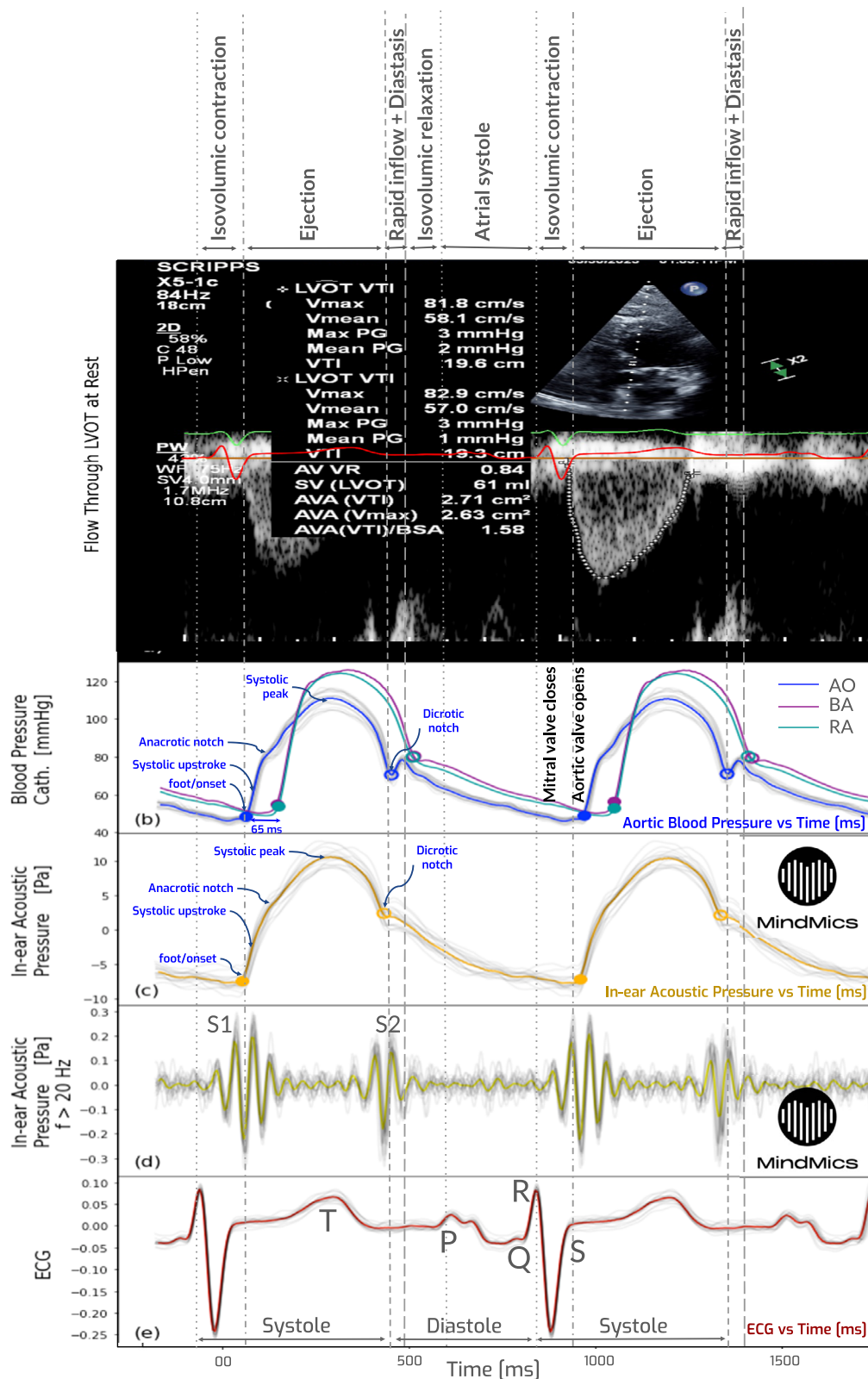
Fig. 1 | Wiggers diagram. Exemplary Wiggers diagram from a clinical study subject CAD23 (82-year-old female; height: 168 cm, weight: 66 kg) with comorbidities including obstructive coronary artery disease and hyperlipidemia. Key cardiac events and intervals are annotated. From top to bottom: **a** Doppler echocardiographic image showing flow through the left ventricular outflow tract (LVOT) at rest; **b** Invasive pressure waveforms from the aorta (blue), brachial artery (purple), and radial artery (dark cyan); **c** In-ear IH waveform corrected for instrumental effects and converted to in-ear acoustic pressure units (yellow); **d** In-ear IH waveform filtered above 20 Hz, highlighting the presence of S1 and S2 heart sounds (yellow); **e** 12-lead electrocardiogram (ECG) tracings (red). The x-axis represents time in milliseconds, with a window covering two cardiac cycles. Full and open circles in panels (**b**, **c**) indicate timings of the AVO and AVC, respectively, reconstructed using algorithms described in the text.
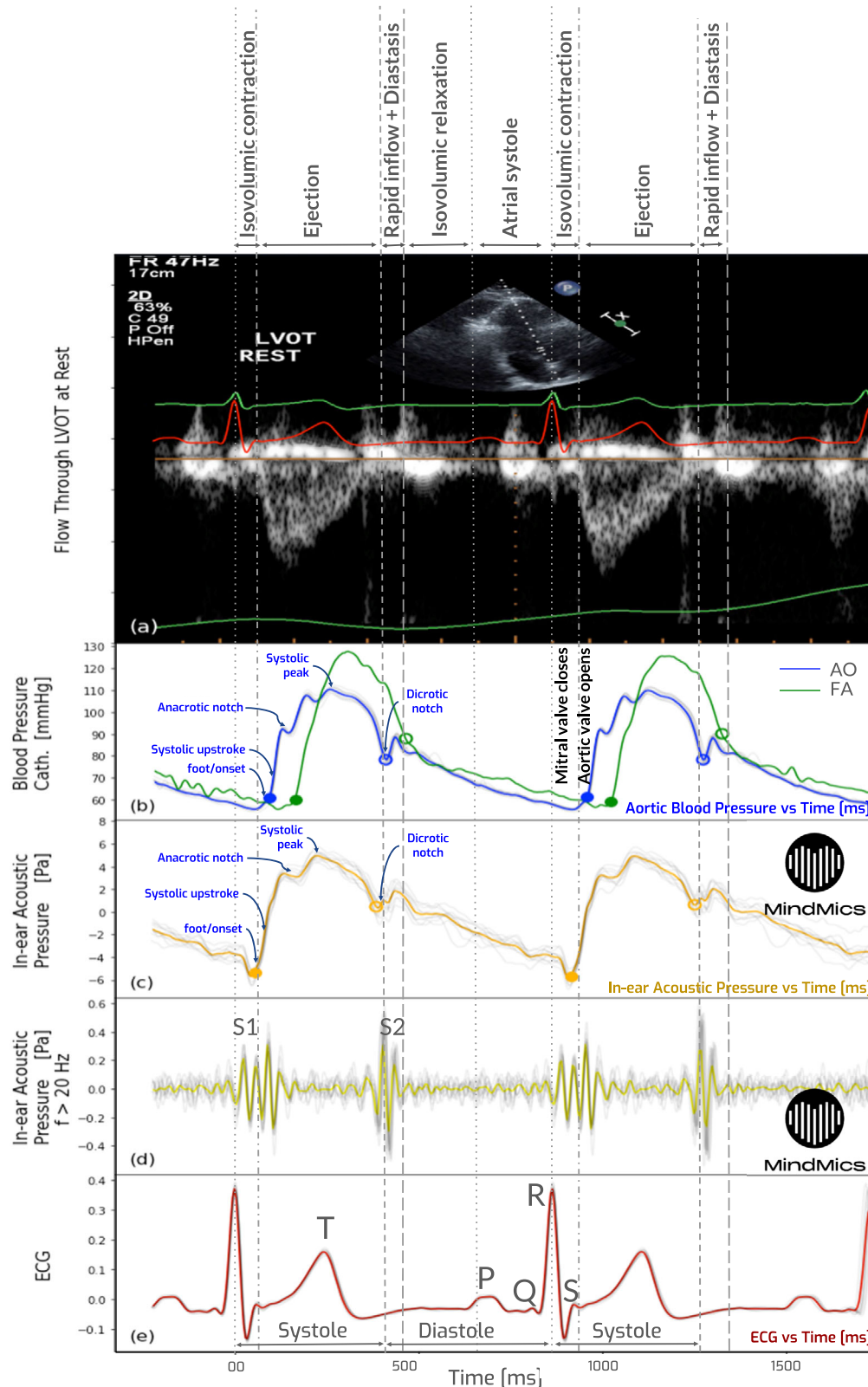
Fig. 2 | Wiggers diagram. Exemplary Wiggers diagram from a clinical study subject CAD06 (64-year-old male; height: 170 cm, weight: 72 kg) with comorbidities including obstructive coronary artery disease, hypertension, hyperlipidemia and diabetes. Key cardiac events and intervals are annotated. From top to bottom: **a** Doppler echocardiographic image showing flow through the left ventricular outflow tract (LVOT) at rest; **b** Invasive pressure waveforms from the aorta (blue), and the femoral artery (green); **c** In-ear IH waveform corrected for instrumental effects and converted to in-ear acoustic pressure units (yellow); **d** In-ear IH waveform filtered above 20 Hz, highlighting the presence of S1 and S2 heart sounds (yellow); **e** 12-lead electrocardiogram (ECG) tracings (red). The x-axis represents time in milliseconds, with a window covering two cardiac cycles. Full and open circles in panels (**b**, **c**) indicate timings of the AVO and AVC, respectively, reconstructed using algorithms described in the text.
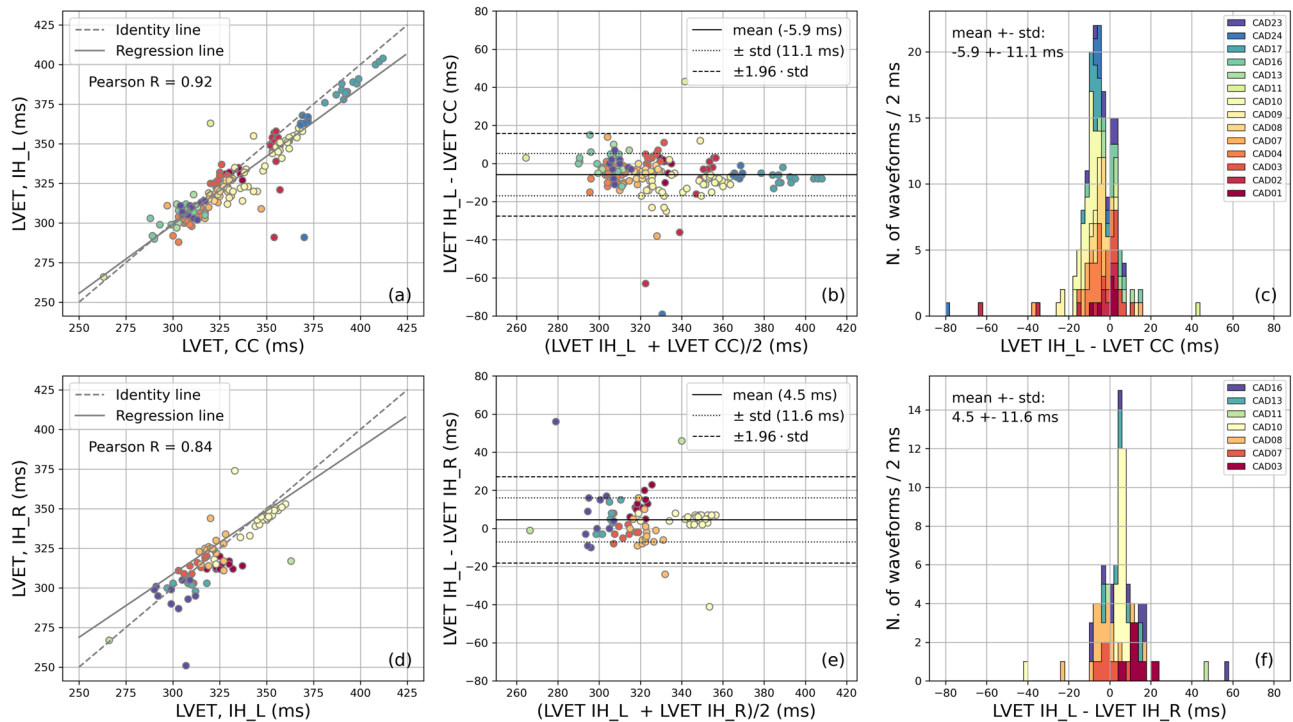
Fig. 3 | LVET comparison. a LVET measured from IH waveforms vs catheter waveforms averaged over 10 consecutive cardiac cycles for 14 study subjects with signals simultaneously detected in the left IH earbud, b the relationship of agreement (Bland-Altman plot), and c the histogram of the difference between LVET measured from both sources; d LVET extracted from IH waveforms using signals from the Left vs Right earbud averaged over 10 consecutive cardiac cycles for 7 subjects with signals detected in both earbuds, e the relationship of agreement (Bland-Altman plot), and f the histogram of the difference between LVET measured from both sources.

associated with the peak rate of pressure increase, is visible in both signals. Following the systolic peak, the dicrotic notch—marking the closure of the aortic valve—is identifiable in the IH waveform as a small inflection, often followed by the dicrotic wave or peak, which reflects diastolic pressure oscillations. The waveform foot, denoting the onset of ventricular ejection, is also detectable in IH recordings and serves as an important timing reference, marking the opening of the aortic valve. These fiducial points are consistently observed across subjects and are annotated in Figs. 1 and 2 for illustrative purposes.

The agreement between IH and CC waveform morphology, quantified using cross-correlation, was 0.997 for the subject in Fig. 1 and 0.976 for the subject in Fig. 2. A similar cross-correlation value of 0.95 was observed when averaging over waveforms in the entire sample of 2,171 cardiac cycles from 18 subjects (see Supplementary Figs. 1 and 2 for complete set of Wiggers Diagrams). These high correlation values indicate a strong consistency between the IH in-ear signals and invasive aortic pressure measurements, underscoring the potential of IH technology to reliably capture and reflect key hemodynamic events in a non-invasive manner.

Timing of the aortic valve opening and closing
The data indicate good agreement in the timing of aortic valve opening (AVO) and aortic valve closure (AVC) between IH and CC measurements. The time between AVO and AVC, known as the left ventricular ejection time (LVET), is a critical parameter in cardiac function assessment. We developed algorithms to detect AVO and AVC to calculate LVET. Timings of AVO and AVC were reconstructed from positions of the maxima of the second derivative of pressure waveforms, convoluted with a Gaussian filter of a width of 13 ms to reduce signal fluctuations. AVO (AVC) was selected as the timing of the most significant maximum of the derivative before (after) the peak of the original waveform, with a significance score calculated taking into account amplitudes of the original signal and its second derivative and the distance from the peak of the original waveform. LVET was then calculated as a difference in time between AVC and AVO. When applied to IH and CC data from 14 study subjects with available left earbud signals, these algorithms

showed a high correlation (r = 0.92, p < 0.0001) between LVET measured from IH and CC (Fig. 3a–c). The standard deviation of the difference between IH and CC measurements was 11.1 ms, with a bias of −5.9 ms (mean ± SEM of 335.1 ± 2.2 ms for CC and 329.2 ± 2.0 ms for IH). A similar correlation was observed for LVET measured simultaneously using IH signals from the left and right earbuds in 7 subjects, with a standard deviation of the difference of 11.6 ms and a bias of 4.5 ms (Fig. 3d–f).

The heart's valves play a crucial role in directing blood flow in a synchronized, one-way pattern between chambers. Proper valvular function produces the characteristic heart sounds S1 and S2, associated with valve closures that mark key moments in the cardiac cycle. Valvular defects can disrupt this flow: regurgitant valves fail to prevent backward flow, while stenotic valves obstruct blood movement into the next chamber. Such defects can create murmurs—audible sounds of turbulent blood flow—that aid in diagnosing cardiac pathology. Typically, systolic murmurs indicate issues with blood exiting the ventricle (e.g., mitral regurgitation, aortic stenosis, hypertrophic obstructive cardiomyopathy), while diastolic murmurs are associated with blood entering the ventricles (e.g., mitral stenosis, aortic regurgitation). Intriguingly, IH signals analyzed at frequencies above 20 Hz reveal acoustic signatures that correspond to the timing of S1 and S2 heart sounds. This alignment underscores IH technology's potential to monitor valve function, providing a non-invasive method to assess heart sounds and detect valvular abnormalities[15,16].

The origin of IH signals
A pivotal question in interpreting IH data is identifying the spatial origin of the detected acoustic signals. whether these sounds originate from the aorta—propagating through the body to the ear canal—or if they emanate from arteries in close proximity to the ear canal.

To address this question, we designed and constructed a proprietary hardware system capable of synchronizing raw data across multiple streams—including IH, CC, and ECG—with millisecond resolution. Time synchronization was achieved by aligning the positions of the QRS peaks from the same ECG signal recorded across all devices.

Article

In evaluating the delay between waveforms, we focused on the timing of the AVO relative to the ECG R peak. We deliberately chose not to use the systolic peak as a reference point because it is primarily influenced by lower-frequency components, which can be disproportionately affected by instrumental effects such as acoustic leakage. These effects could mimic a delay, making the systolic peak less reliable for precise timing comparisons.

In our data, the average measured AVO appears 96.7 ± 11.4 ms and 98.3 ± 16.9 ms (mean $\pm$ SD) after the R wave of the ECG for CC and IH waveforms, respectively. An unpaired t-test indicated no statistically significant difference between the two measurements, (t(34) = −0.34, p = 0.74).

The absence of a visible delay in the IH signal relative to the CC signal suggests that IH detects sound waves originating directly from the heart and aorta. These sound waves propagate through the human body at a speed of ~150 cm/ms[31]. The average distance between the heart and the ear in a typical adult is ~30 cm, assuming a straight-line path from the left ventricle of the heart to the ear canal[32,33]. Therefore the sound waves can cover the average distance in merely 0.2 ms. In contrast, if the IH signal originated from the carotid arteries near the ear canal, given an average pulse wave velocity of 0.35 cm/ms[34] and a propagation length of about 30 cm between the heart and the ear, we would expect a delay of ~86 ms relative to the catheter signal, which is not observed. In evaluating the expected delay, we also considered age-matched aortic pulse wave velocity (AoPWV) values representative of individuals aged 60–75 years, with the mean AoPWV of 0.87 ± 0.23 cm/ms in individuals without hypertension or diabetes, and 1.02 ± 0.25 cm/ms in those with either condition[35]. Assuming a heart-to-ear path length of 30 cm, this corresponds to an expected pulse transit delay of ~29–34 ms, which is also not observed. The difference between AVO timings from IH and CC was 1.6 ± 12.1 ms. This minimal difference allows us to reject the hypothesis that the IH signal originates from the carotid arteries near the ear with a significance greater than 7 and 3 standard deviations assuming the PWV reported in ref. 34 and ref. 35, respectively.

The interval between the R wave on the ECG and the AVO represents the isovolumetric contraction time (IVCT). The peak of the R wave on the ECG marks the onset of ventricular systole and corresponds to the initial myocardial contraction that contributes to the first heart sound and mitral valve closure[36]. This early systolic phase can also be assessed via echocardiography as the interval between mitral valve closure and aortic valve opening. In the general population, IVCT typically ranges from 30 to 50 ms[37–40]. However, IVCT is known to prolong in subjects with elevated risk of heart failure (HF) as an example. For instance, ref. 41 reported a 24% increase in HF risk for every 10 ms increase in IVCT. Additionally, ref. 42 observed that IVCT was prolonged to 90 ms in subjects with aortic stenosis and up to 120 ms in those with pulmonary arterial hypertension. Our measurements are consistent with prolonged IVCT, expected for our study subject population.

To further test the origin of the IH signal, we compared the expected pulse transit time (PTT) from the heart to the ear with values reported in ref. 43, where photophletysmography (PPG) sensors were used to measure the onset of waveforms corresponding to AVO at multiple peripheral sites, including the ear. In that study, the pulse arrival time at the ear was measured to be ~140 ms after the R peak of the ECG (Fig. 4, ref. 43). In contrast, in our study population, the mean onset of the waveform indicating AVO was 96.7 ± 11.4 ms for catheter-based (CC) waveforms and 98.3 ± 16.9 ms for IH waveforms—representing a substantial deviation from the PPG-based measurements in healthy subjects. An unpaired t-test between PPG-based (mean = 140 ms, SD = 10 ms, n = 116) and our measurement (mean = 98.3 ms, SD = 16.9 ms, n = 18) confirms a highly significant difference between the distributions; t(132) = 16.75, p < 0.0001.

Finally, Fig. 1 clearly demonstrates a delay of ~65 ms in the radial and brachial waveforms relative to the timing of the aortic waveform. This delay is absent in the IH waveform, contrary to what would be expected if the infrasonic signal was caused by the pulse wave in the carotid artery.

Blood pressure prediction

The preceding sections established the central origin of the IH signal and demonstrated the high correlation between aortic pressure gradients and timings obtained from IH and CC measurements. While CC directly measures aortic blood pressure, IH captures dissipated acoustic signals in the ear canal, recorded as in-ear acoustic pressure. As illustrated in the Wiggers diagrams, the acoustic pressure during the systolic peak measured by IH typically ranges from 3 to 15 Pa, corresponding to 0.022 to 0.112 mm Hg. This amplitude is ~1000–5400 times smaller than the typical arterial systolic pressure of 120 mmHg. Despite the high correlation in waveform shape, the amplitudes and baseline of IH signals is inherently variable due to several factors, including instrumental effects such as acoustic leakage caused by ear tip fit, variations in impedance related to respiratory rate, differences in earbud fit, physiological asymmetries between the left and right ears, and other subject-specific anatomical variations. Relying on amplitude for BP predictions would necessitate frequent calibrations to account for these sources of variability, complicating practical implementation.

However, the high fidelity of the IH waveforms and the breadth of extractable cardiac features motivated the hypothesis that BP could be accurately predicted by leveraging amplitude-invariant features derived from waveform shape dynamics and timings of cardiac functions. These dynamics reflect hemodynamic changes associated with BP and influence the morphology of the pressure waveform, including acoustic imprints from valve activity. To test this hypothesis, we removed amplitude information entirely and engineered features that focus solely on waveform morphology to predict SBP and DBP. This approach has the potential to provide medically and commercially valuable metrics while normalizing IH waveforms for further applications in non-invasive aortic pressure monitoring.
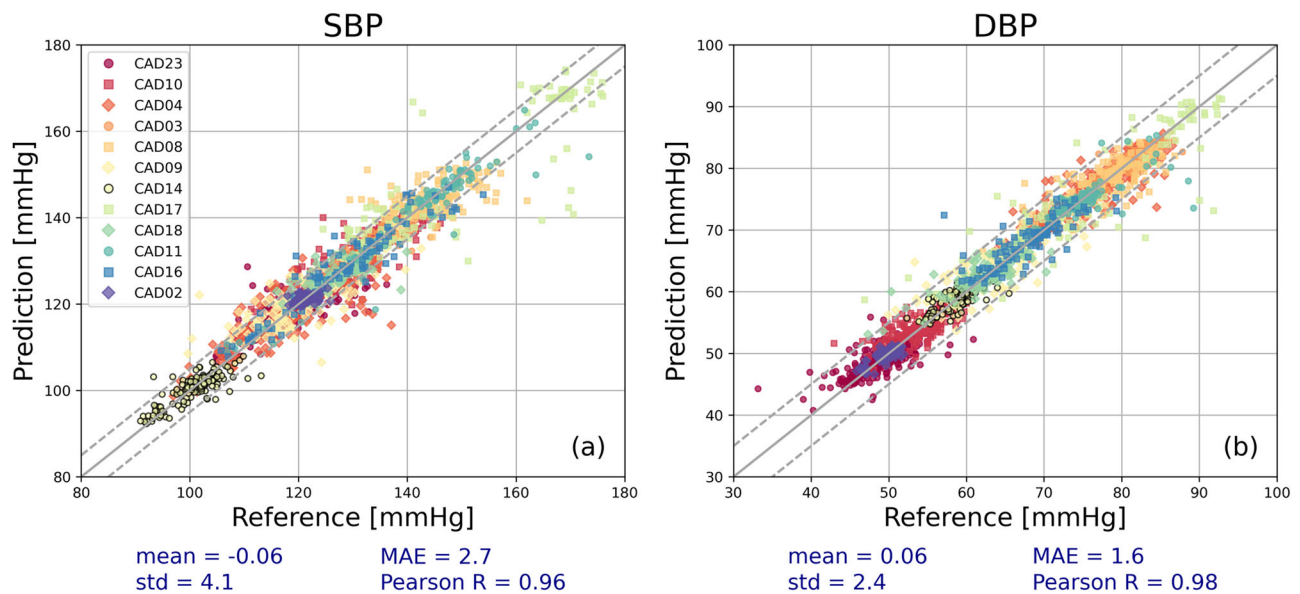
To validate this hypothesis, we performed an analysis predicting SBP and DBP using waveform shape features from both CC and IH signals. Data from 12 subjects were included, with each subject contributing at least 1.5 min (≥90 cardiac cycles) of data to ensure a sufficient number of observations. Reference BP values were obtained from CC measurements, offering precision (~1 mmHg) superior to traditional BP cuff devices. The reference SBP was defined as the maximum of the CC waveform, while the reference DBP was taken as its minimum.

Approximately 30 features were extracted from normalized CC and IH waveforms (amplitudes scaled to [0,1]) for each subject. These features included key timings within the cardiac cycle, such as AVO and AVC, first and second derivatives of the waveform, and other shape-based metrics. Models were trained and validated using 5-fold cross-validation, with Mean Absolute Error (MAE) as the evaluation metric. Results for IH-predicted versus CC-measured BP values are summarized in Figs. 4 and 5, for SBP and DBP predictions. The standard deviations of the differences between predicted and reference BP values averaged across all 12 subjects were 4.1 mmHg (SBP) and 2.4 mmHg (DBP) for CC data, and 5.8 mmHg (SBP) and 3.7 mmHg (DBP) for IH data.

To further evaluate the model's ability to capture rapid physiological changes, we illustrate BP time series for two representative study subjects, as shown in Fig. 6. A study subject in Fig. 6a displayed periodic variations in BP due to respiratory sinus arrhythmia, with predicted systolic and diastolic BP closely replicating these patterns. The study subject in Fig. 6b exhibited rapid changes in systolic BP, fluctuating from 140 mmHg to 115 mmHg over several dozen seconds. In both cases, the models accurately captured these dynamic changes, demonstrating the robustness of the approach.

Figures 4–6 collectively highlight that waveform shape alone, independent of demographic variables, is sufficient for accurate BP prediction within individual subjects. The average prediction error was within 5 mmHg, aligning with clinical standards for BP measurement accuracy. However, the limited sample size of 18 study subjects—even when including those with fewer waveforms—is insufficient to develop a generalized predictive model capable of accounting for inter-individual physiological variability.
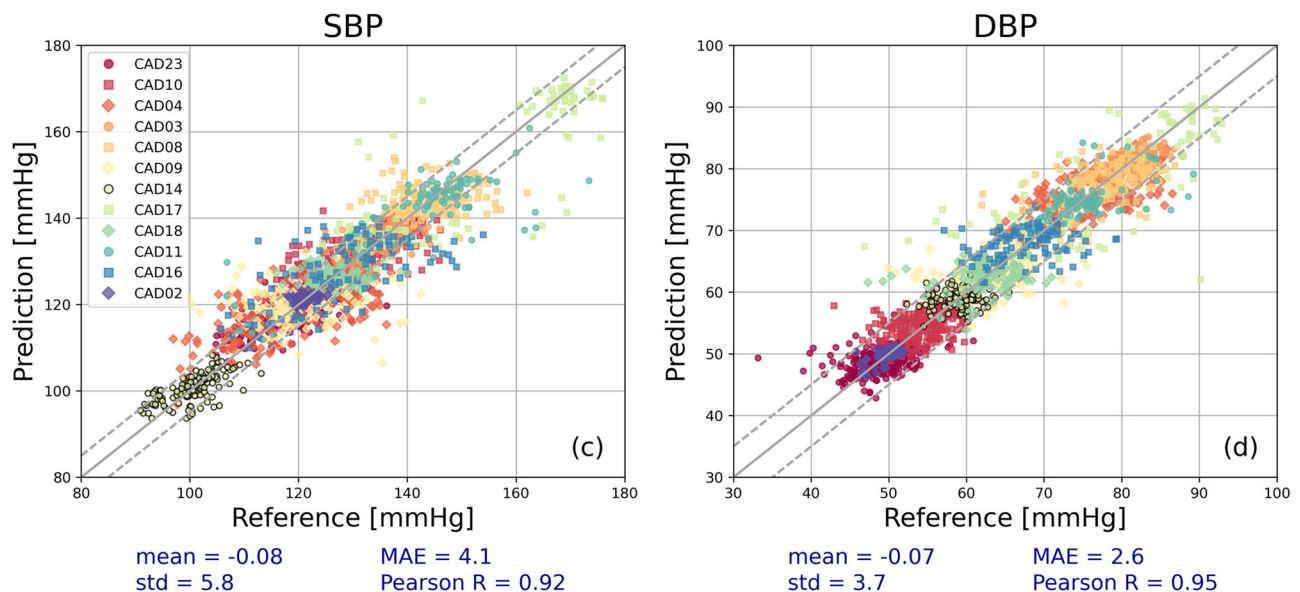
Fig. 4 | BP correlations. Predicted vs measured values of SBP and DBP for the cardiac catheterization (**a**, **b**) and IH (**c**, **d**) data from 12 CAD study subjects. Dashed lines bracket regions corresponding to ±5 mmHg around the identity line (solid line).

To explore the feasibility of a generalized "one model for all," we trained a model using data from all 18 study subjects, including demographic variables. As expected, the model's performance was suboptimal, with standard deviations of prediction errors reaching 16.2 mmHg (SBP) and 8.3 mmHg (DBP) for CC data, and 15.3 mmHg (SBP) and 8.0 mmHg (DBP) for IH data. This reinforces the need for larger, more diverse datasets to generalize BP predictions effectively.

Interestingly, when we seeded the training set with five data points from the test subject, the model demonstrated substantial improvement in prediction accuracy. Under this approach, standard deviations of prediction errors were reduced to 8.6 mmHg (SBP) and 4.8 mmHg (DBP) for CC data, and 9.8 mmHg (SBP) and 5.7 mmHg (DBP) for IH data. These results suggest that integrating even a minimal amount of data with familiar physiology could enhance the model's ability to generalize across diverse populations.

In conclusion, the results demonstrate that BP information is encoded in pressure waveform shape dynamics, and the current feature set is sufficient for accurate BP prediction within individual subjects. The strong agreement between IH-predicted and CC-measured BP, positions the IH technology as a promising tool for non-invasive aortic pressure monitoring and dynamic BP assessment. With larger and more diverse datasets, this approach could support the development of robust, generalizable BP prediction models for widespread clinical and consumer applications.

Discussion

This study demonstrates the potential of IH as a non-invasive technology for capturing and interpreting detailed cardiovascular hemodynamics. The strong alignment between IH waveforms and invasive aortic pressure measurements, as depicted in the Wiggers diagrams, indicates that IH can
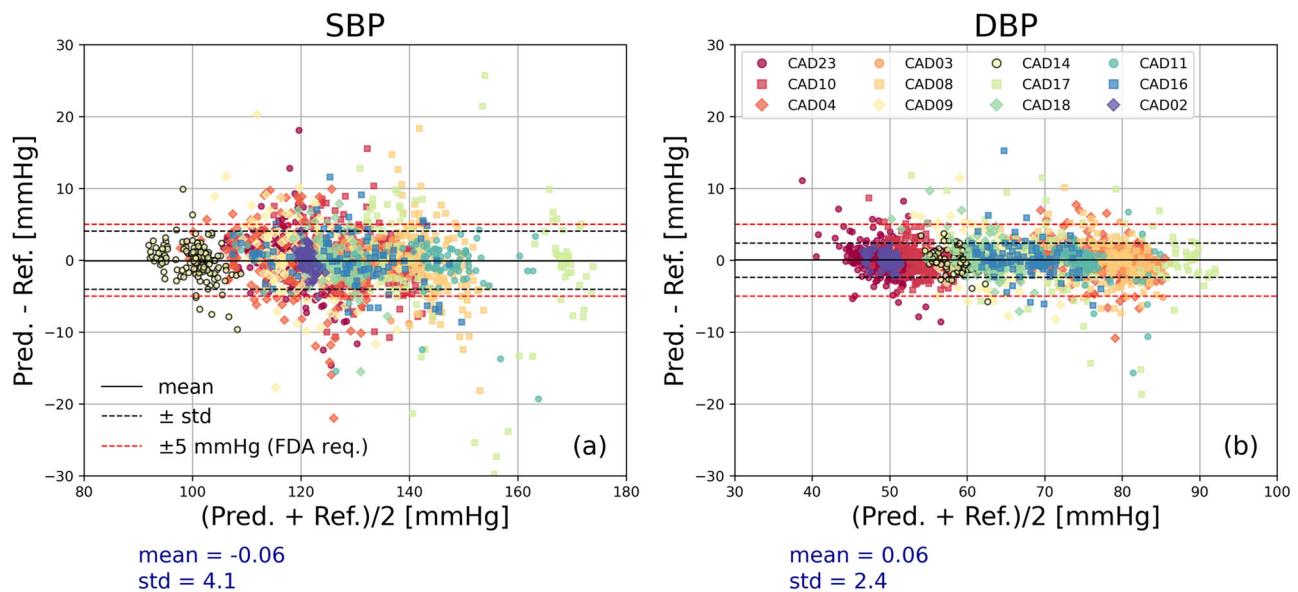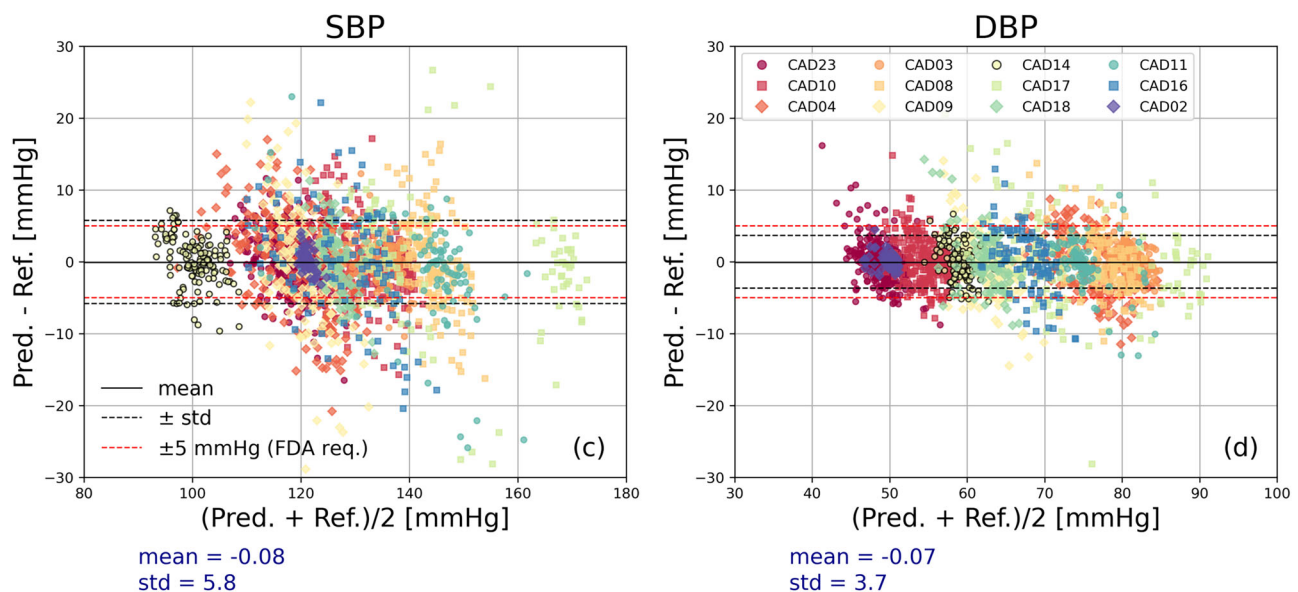
Fig. 5 | Bland–Altman plots. The relationship of agreement for predicted and measured values of SBP and DBP for the cardiac catheterization (**a**, **b**) and IH (**b–d**) data from 12 CAD study subjects. Solid and dashed black lines correspond to the mean value and the standard deviation of the difference between predicted and measured BP values. Dashed red lines represent the region of ±5 mmHg around the mean.

represent key hemodynamic events of the cardiac cycle. The high cross-correlation values (mean r = 0.95) between normalized IH and CC waveforms underscore this capability.

A key finding of this research is the confirmation that the primary component of the IH signal in a study subject at rest originates from central cardiac activity. By synchronizing IH, CC, and ECG data with millisecond precision and analyzing the timing of the AVO, we established that the major component of the IH signals originate directly from the heart and aorta rather than from peripheral arteries near the ear canal. The minimal difference in AVO timings between IH and CC measurements 1.6 ± 12.1 ms effectively rejects the hypothesis of a peripheral arterial origin. This insight not only validates the physiological basis of IH technology but also enhances its feasibility for clinical applications.

The study further explores the feasibility of predicting systolic (SBP) and diastolic (DBP) blood pressure using waveform morphology independent of amplitude. The infrasonic nature of the technology brings novel challenges to using the amplitude directly that can be influenced by variability due to factors like acoustic leakage, earbud fit, and study subject-specific anatomical differences. By engineering amplitude-invariant features derived from the waveform morphology and cardiac timing events, we demonstrate blood pressure predictions with the standard deviations of the differences between predicted and reference BP values averaged across 12 subjects to be 4.1 mmHg (SBP) and 2.4 mmHg (DBP) for CC data, and 5.8 mmHg (SBP) and 3.7 mmHg (DBP) for IH data.

The ability of IH technology to detect acoustic signatures corresponding to heart sounds S1 and S2 adds another dimension to its diagnostic potential. In concept, IH could also detect S3, and exhibits a possible
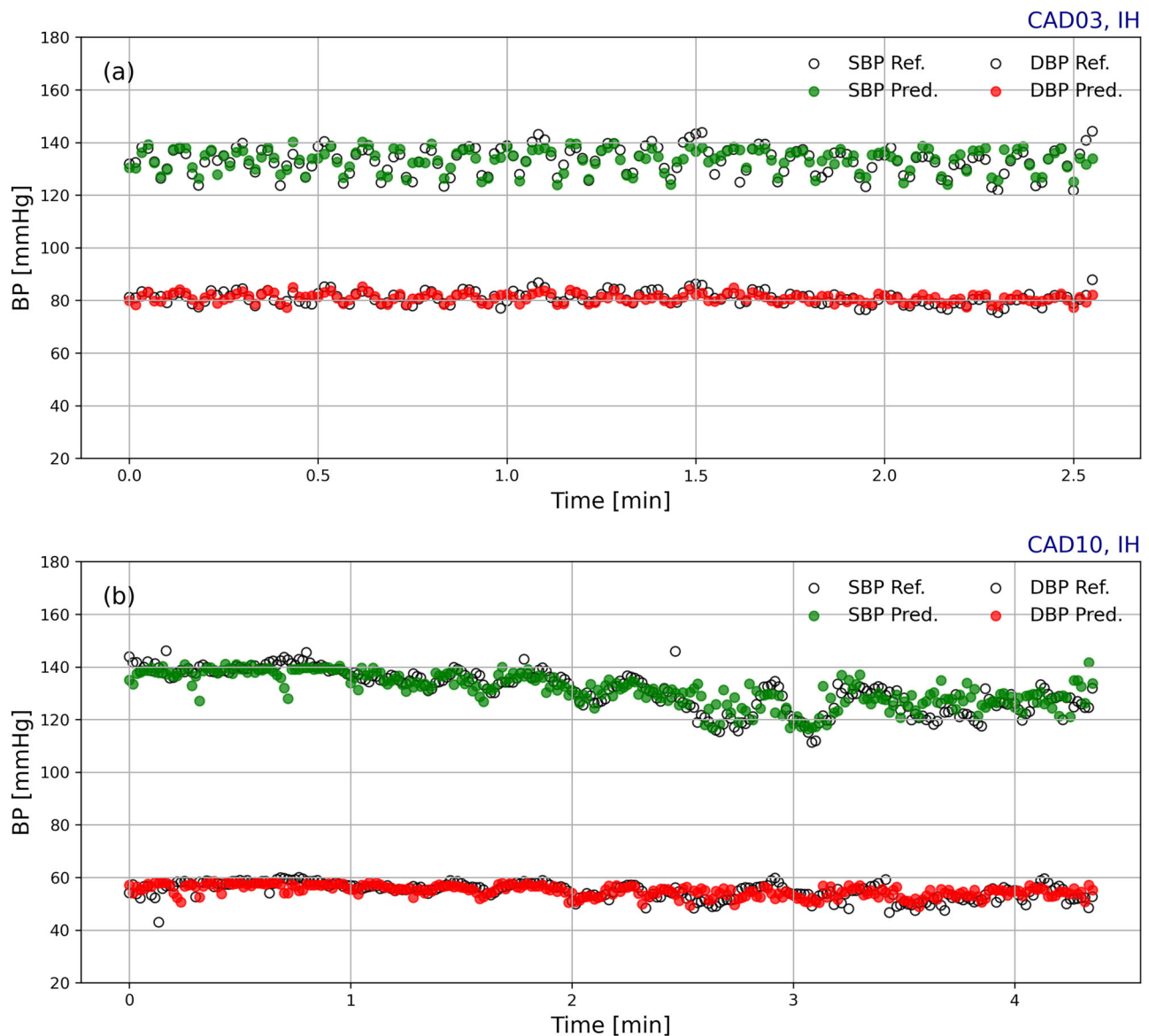
Fig. 6 | Time dependence of BP predictions. Predicted values of SBP (solid green) and DBP (solid red) using Gradient Boosting Model (GBM) model and IH data from two exemplary study subjects: **a** CAD03 and **b** CAD10, shown as a function of measurement time and compared to reference SBP and DBP values (open black) extracted from simultaneously recorded catheter waveforms.

S4 component in CAD02 (see Supplementary Fig. 1) a sign of elevated left ventricular filling pressures in study subjects with decompensated heart failure, and it has already been shown that IH can detect systolic murmurs in a study subject with severe aortic stenosis[15]. This feature enables the non-invasive monitoring of valve function and the detection of valvular abnormalities, such as murmurs resulting from regurgitant or stenotic valves. Such capabilities could significantly enhance early detection and management of cardiac pathologies.

Despite these promising results, the study has limitations that warrant consideration. The sample size was 18 study subjects with limited degrees of cardiac and non-cardiac pathology, which can not represent the diversity of physiological variations in the broader population. While individual models showed high accuracy, attempts to develop a generalized "one model for all" support the need for larger and more diverse datasets. Future studies should aim to include a broader demographic to improve model generalizability.

Another limitation is the focus on study subjects undergoing CC for coronary artery disease evaluation. On the positive side, it demonstrates the feasibility of the technology in a population that stands to benefit most from accurate blood pressure monitoring—individuals with severe symptoms or pre-existing heart conditions, rather than in a typical, healthy cohort. However, the drawback lies in the limited generalizability of the findings to broader patient populations or alternative clinical settings. Longitudinal studies evaluating the performance of IH technology across a range of clinical conditions and over extended periods will be invaluable for assessing its robustness, reliability, and broader applicability.

In conclusion, this study establishes IH technology as a promising tool for non-invasive cardiovascular monitoring. By accurately capturing central hemodynamic events and enabling blood pressure prediction based on waveform morphology, IH has the potential to transform patient care. With further research and larger datasets, IH technology could support the development of robust, generalizable models suitable for widespread clinical and consumer applications, ultimately contributing to improved cardiovascular health management.

The physiological origin of in-ear cardiac acoustic signals has been the focus of several recent studies, with differing interpretations. Some have suggested that these signals result from compressive waves conducted from the heart to the ear canal[44–46], while others propose local arterial expansion

near the ear as the source[47–49]. Reference [50] contributed to this discussion by showing that both mechanisms may play a role, based on multimodal signal analysis.

Our study enables us to further clarify the physiological source of in-ear acoustic signals by incorporating gold standard medical devices including CC and ECG as a timing reference. By synchronizing CC waveforms with ECG, and IH, we were able to align signals against precise cardiac events—specifically, AVO. This approach was especially important in our population, which includes individuals with prolonged IVCT, where delays of 30–60 ms could confound interpretations based solely on non-invasive timing. Our results support the view that, in resting study subjects, the IH signal is predominantly of aortic origin, as evidenced by its strong temporal and morphological correlation with aortic pressure waveforms. However, multiple physiological mechanisms may contribute to in-ear cardiac acoustics, with the ear functioning as an integrative biosensor.

The ear serves not only as a sensory organ for hearing but also as a sophisticated transducer, capable of capturing and transmitting low-frequency vibrations originating from various organs and bodily movements. These vibrations, generated by physiological processes such as cardiac activity, blood flow, respiration, and musculoskeletal movements, propagate through the body's tissues, bones, and arteries, ultimately being detected by the ear. This transduction capability provides a unique opportunity to acquire valuable insights into the body's internal physiological processes.

Unlike a stethoscope, which requires precise placement on specific areas of the body to capture localized sounds, the ear functions as a natural biosignal integrator. It is capable of picking up vibrations from multiple sources simultaneously without the need for exact placement. The stethoscope is constrained by the necessity of skilled technicians positioning the instrument correctly to obtain accurate readings, a limitation that is not present with the ear. The ear, being consistently positioned on the head, maintains a relatively constant distance to key sources of vibrations, making it an ideal sensor for continuous, non-invasive monitoring.

In this study, we focused on pressure waveforms obtained while study subjects were at rest, minimizing the contribution of biosignal originating from body motion. As a result, the biosignal was dominated by the origin from the central cardiovascular system, as indicated by their strong correlation with aortic waveform tracings. However, the ear canal integrates signals from multiple sources, and contributions from the carotid arteries or intracranial pressure are plausible. These signals likely have significantly lower amplitudes, as more prominent delayed components would otherwise be evident. Enhancing microphone sensitivity, reducing their noise floor, and developing more advanced algorithms will be essential to disentangle these signals from other biosignals originating from different parts of the cardiovascular system or even other organs, such as the brain or digestive system. This approach could pave the way for comprehensive, multimodal non-invasive monitoring.

In-ear blood pressure monitoring offers significant advantages due to its ease of use and integration with existing habits. For cardiac care, measuring blood pressure just twice daily could provide valuable data to healthcare professionals, enabling better management of medication dosages and treatment plans. Additionally, giving patients direct access to their blood pressure data reinforces lifestyle changes by helping them see the immediate impact of their choices on their cardiovascular health. This real-time feedback can promote healthier habits and make the consequences of negative behaviors more evident.

The combination of IH technology with wellness systems, such as those offering stress reduction protocols or breathwork exercises, could be particularly powerful. By giving patients tools to explore how their actions affect blood pressure, they can learn to manage their health more effectively, gaining insights into which behaviors raise or lower their blood pressure.

Blood pressure level is often affected by diurnal variation, such as stress, physical movement, or emotional state. These factors can temporarily raise blood pressure, which may be a healthy physiological response but could lead to misdiagnosis if the readings are not contextualized. IH technology, integrated into earbuds that frequently contain motion sensors (Inertial Measurement Units, IMUs), can address this issue by providing context to each measurement. The IMUs can detect motion levels before and during blood pressure readings, helping determine whether the patient was active or at rest.

Additionally, IH can measure heart rate (HR) and heart rate variability (HRV), offering further insights into whether the patient was relaxed or stressed at the time of the measurement. This contextual data could allow healthcare providers to distinguish between normal physiological responses and genuine hypertension, improving diagnostic accuracy and reducing unnecessary medication. Moreover, the ability to measure blood pressure in a relaxed, home environment can mitigate the effects of "white coat syndrome", where patients experience elevated readings in clinical settings. This approach offers higher accuracy by eliminating patient-dependent factors such as technique, cuff size, and other technical limitations associated with standard cuff-based measurements.

In addition to its applications in blood pressure monitoring, IH technology holds significant promise for a variety of clinical and consumer uses. One notable area is arrhythmia detection. Building on recent advancements in wearable technology, IH can enhance this capability by reducing false positives and enabling detection in asymptomatic populations. Furthermore, exploring the impact of irregular heart rhythms on hemodynamics could lead to new biomarkers for assessing the severity of atrial fibrillation. This has the potential to improve stroke risk assessments, support the study of anticoagulant treatments, and enhance patient adherence and compliance.

These advancements are especially valuable for continuous, at-home monitoring, reducing the need for invasive procedures such as Holter monitoring. Additionally, IH's ability to monitor heart function opens new avenues for detecting and managing valvular heart disease and heart failure, enabling ongoing, remote assessment of these conditions. As IH technology evolves, its integration into fitness and wellness applications will also grow, offering a more comprehensive approach to cardiovascular health.

These developments position IH as a versatile tool for both preventive and therapeutic cardiac care.

The future of preventive cardiac care will be driven by AI and real-time data from wearable devices like in-ear sensors. IH technology, combined with AI, enables continuous cardiovascular monitoring, allowing for early detection of hypertension, arrhythmias, and other conditions. This shifts healthcare from reactive to preventive, empowering clinicians to intervene before critical events occur. AI algorithms, trained on high fidelity datasets, will enhance precision by identifying subtle patterns missed by traditional methods, enabling personalized treatment plans tailored to each patient's unique cardiovascular profile and combining it with lifestyle and wellbeing solutions.

The success of this approach relies heavily on robust, secure cloud infrastructures. Real-time, closed-loop systems—where wearable devices continuously collect data, transmit it to the cloud for analysis, and provide feedback—require high levels of data security. Ensuring that data is encrypted, securely stored, and processed in compliance with privacy regulations (e.g., HIPAA, GDPR) is essential to maintaining trust and safeguarding sensitive health information. These systems can enable immediate adjustments to care, such as medication changes or lifestyle recommendations, based on AI-driven analysis of real-time data, transforming preventive cardiac care by delivering timely interventions, reducing hospitalizations, and improving outcomes.

As a feasibility study, our primary aim was to evaluate the potential of IH for non-invasive cardiovascular monitoring under controlled clinical conditions. While the results are encouraging, several limitations inherent to the study design and population should be considered when interpreting the findings and planning subsequent validation efforts. The results presented in this study were obtained using a prototype device in which the earbuds were connected to a controller board via cables. Additional connections linked the controller board to an ECG device, a GE system, and a data acquisition computer. This setup introduced sensitivity to external

vibrations, as movements or environmental factors could propagate through the cables to the earbuds. In many instances, non-stationary signals —often generated by study subject motion or background noise—exhibited amplitudes significantly higher than the cardiac signals, occasionally even saturating the system.

Data collection in a cardiac catheterization lab (cath lab) posed additional challenges due to the inherently dynamic environment. Frequent adjustments to the patient bed, imaging equipment, and other tools necessary for optimizing catheter placement introduced further motion and vibration. These factors complicated the collection of clean, and high-quality data.

The analysis focused on demonstrating the potential of IH technology for blood pressure prediction, specifically targeting periodic heartbeats from study subjects lying on cath beds. To minimize motion-related noise, study subjects were sedated to maintain a state of rest. However, a comprehensive analysis of motion-related signals—such as those generated by walking, eating, or other activities—was not feasible given the constraints of the cath lab setting and is beyond the scope of this paper.

Several limitations should be considered when interpreting these results:

1. Small sample size: The study involved only data from 18 subjects, which may lead to an overestimation of the accuracy of systolic (SBP) and diastolic (DBP) predictions, as well as the observed correlation between IH and cardiac catheterization (CC) measurements. The limited number of study subjects restricts the statistical power of the study and may not capture the full range of physiological variability present in the general population.

2. Narrow blood pressure range: Measurements were primarily taken while study subjects were at rest and under sedation, resulting in a narrow range of blood pressure values. Changes in blood pressure were mainly driven by study subject physiology at rest, which may not reflect the fluctuations that occur during daily activities or stress conditions.

3. Study subject population focus: The study concentrated on patients undergoing CC for coronary artery disease evaluation. This focus has both advantages and disadvantages. On one hand, it demonstrates the feasibility of the technology in a population that stands to benefit most from accurate blood pressure monitoring—individuals with severe symptoms or pre-existing heart conditions. On the other hand, this specificity limits the generalizability of the findings to broader study subject populations or alternative clinical settings. The physiological characteristics of study subjects with coronary artery disease may differ from those of the general population.

4. Data collection constraints: The cath lab environment imposed significant constraints. Short recording durations for aortic blood pressure—necessitated by patient safety considerations and the primary clinical objectives of the procedure—resulted in variable amounts of data collected per study subject. This limitation affected our ability to generate individualized blood pressure predictions for many study subjects, as there was insufficient data for model training in several cases.

5. Variability in data quality and quantity: The variability in the number of data points between study subjects, combined with the small sample size, made it difficult to create a statistically robust model applicable to all. Large inter-individual physiological differences, such as variations in ear canal anatomy, tissue composition, and cardiovascular health status, further restricted our ability to build a generalized model. Blood pressure changes were often outweighed by study subject physiological differences, complicating efforts to accurately reflect diverse study subject populations.

6. Prototype device limitations: The reliance on a prototype device introduces several limitations: a) Earbud Fit and Seal: Proper earbud fit and seal are important for accurate IH signal detection. Variations in ear canal anatomy and differences in earbud placement can affect signal quality, introducing additional variability. b) Technical Limitations: The prototype may not fully represent the performance of a finalized commercial product. c) Ambient Noise and Interference: Ambient noise and electromagnetic interference within the cath lab may have impacted signal quality. While efforts were made to minimize these factors, complete elimination was not possible.

7. Short-term study duration: The study captured data over short periods during medical procedures. Long-term reliability and consistency of IH technology for continuous monitoring remain unverified. Extended studies are needed to assess device performance over time, including potential drifts in sensor accuracy and the impact of prolonged use on signal quality.

To address these limitations, future studies should expand the sample size to include a larger and more diverse population, enhancing statistical power and generalizability. Incorporating varied study subject populations, such as healthy individuals and those with different cardiovascular conditions, will help assess the technology's applicability across broader groups. Real-world testing under daily activities involving motion and varying environmental conditions is necessary to simulate practical use. Longitudinal studies are needed to evaluate the consistency of IH technology over time, identifying potential issues like sensor drift or user compliance. Advancing device design toward wireless, miniaturized versions would reduce susceptibility to external vibrations and enhance user-friendliness. Addressing these areas will further validate IH technology as a non-invasive, accurate tool for continuous blood pressure monitoring and cardiovascular health assessment.

Methods

In-ear IH, occlusion and acoustic leak

In-ear IH technology captures biosignals as fluctuations in pressure inside the ear canal, measured against a reference like ambient atmospheric pressure. These biosignals are primarily in the infrasonic range (0–20 Hz), frequencies below the audible spectrum (20–20,000 Hz). This low-frequency range, often less susceptible to ambient noise, contains valuable physiological information.

The IH earbud, with an in-ear placement design, not only plays audio but also detects biosignals in the infrasonic range. Each IH earbud includes a microphone for detecting pressure changes, as shown in Fig. 7. After applying proprietary algorithms to correct for instrumental effects and frequency response associated with the earbud placement in the ear canals[51], the device response function is flat in frequency down to fractions of Hz, with the manufactured microphone sensitivity of -37 ± 1 dB and device tolerances within 6 dB at 1 Hz. Accurate detection relies on a seal between the ear tip and the ear canal wall, which introduces the occlusion effect: by blocking the ear canal, it creates a closed acoustic cavity that significantly amplifies internal sound pressure, particularly at low frequencies[9].

This amplification effect can be explained using Boyle's ideal gas law, where pressure and volume are inversely related. By sealing the ear canal even partly, the effective acoustic volume decreases sharply, resulting in a corresponding increase in dynamic acoustic pressure. This amplification can reach up to 40 dB, equating to a 1000-fold increase in amplitude, when the ear canal's volume is reduced from an open 200 cc to a tightly sealed 2 cc. If the volume shrinks by half, it can boost biosignal strength by ~6 dB. This amplification is highly dependent on the level of the seal. Any acoustic leak—a small gap between the ear tip and the canal wall—compromises the seal, reducing the impedance and allowing low-frequency energy to escape. This leak decreases the dynamic pressure, lowering the occlusion effect and, therefore, the sensitivity of biosignal detection. Variations in earbud seals change the sensitivity of IH technology to detect biosignals across different frequencies, causing significant changes in both the amplitude and waveform shape, due to the frequency-dependent nature of impedance changes, which require proper instrumental corrections[51].

Data collection protocol

The data sample used in this work was recorded in a clinical study at Scripps Health (ClinicalTrials.gov Identifier: NCT04636892; start date:

Fig. 7 | IH earbud positioned in the ear canal and with an exploded view of internal earbud components. The seal between **a** the ear tip and the canal wall is critical for achieving occlusion and minimizing acoustic leakage of infrasonic biosignals. The earbud consists of **b** a flexible silicone boot for comfort, mounted on **c** a front cap that houses **d** a MEMS microphone with sufficient sensitivity to detect infrasound. The rear section comprises **e** a speaker ring supporting **f** a speaker enclosed in **g** a back cap. Together, these components enable full-range audio playback. The system interfaces via **h** a cable connected to **i** PCB board integrated with the clinical data acquisition setup. **j** Audio playback can occur in **k** the ear canal simultaneously with **l** biosignal monitoring, as infrasonic biosignals (<20 Hz) occupy a frequency range below that of audible sound (>20 Hz), allowing both functions to operate concurrently without interference. All components are off-the-shelf. Earbud design by MindMics, Inc.
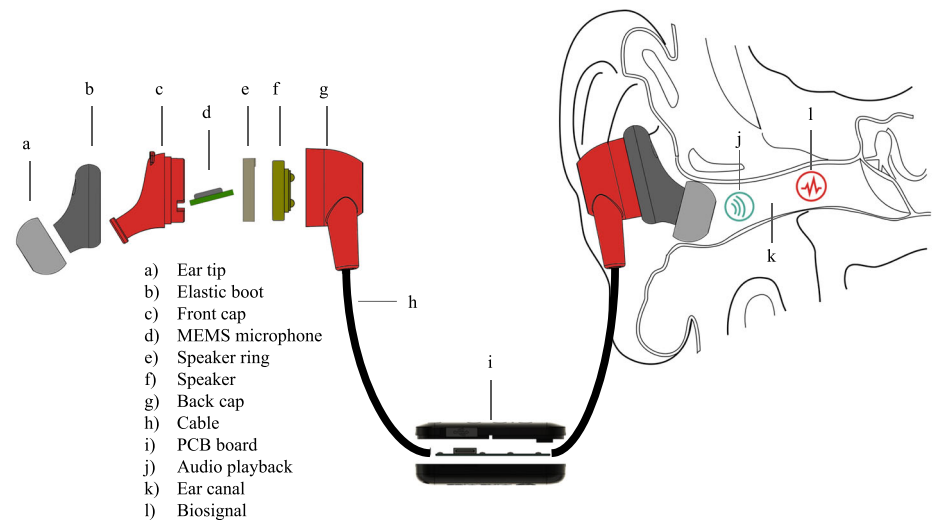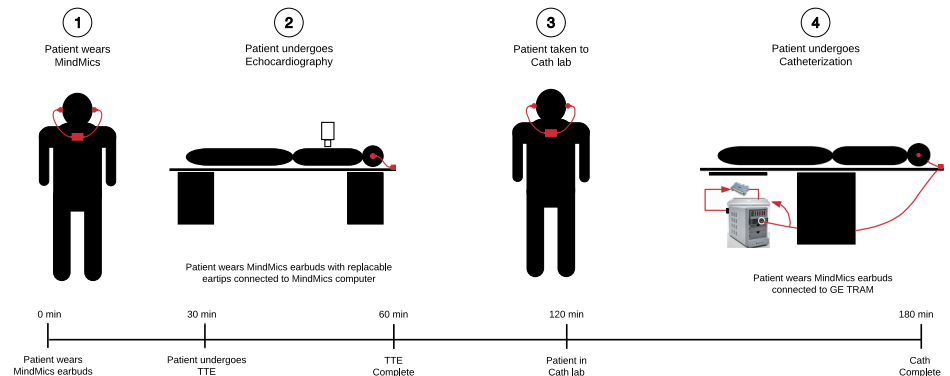

a) Ear tip
b) Elastic boot
c) Front cap
d) MEMS microphone
e) Speaker ring
f) Speaker
g) Back cap
h) Cable
i) PCB board
j) Audio playback
k) Ear canal
l) Biosignal

Fig. 8 | Clinical setup. Clinical setup for data collection using TTE, LHC, ECG, and IH.

Jan 5, 2021, end date: June 13, 2023, approved by Scripps Health Institutional Review Board) from 24 study subjects undergoing in-vivo CC for evaluation of the coronary artery disease (CAD). Among 5 groups of cardiovascular diseases enrolled in the study, the CAD study subjects exhibit aortic waveforms consistent with those of healthy individuals, providing good representation of the target population. The data collection protocol involved recording of simultaneous signals from MindMics earbuds and gold-standard cardiac monitoring devices: electrocardiogram (ECG), pulsed wave Doppler echocardiogram, and cardiac catheter. The goal of the study was to determine the accuracy and validate the IH technology for hemodynamic and cardiac measurements using gold-standard signals. Locally, the project was coordinated by 3 cardiologists and 2 clinical trial coordinators (CTC) at Anderson Medical Pavilion, Scripps Health, La Jolla, CA. Three areas were used for protocol activities, as depicted in Fig. 8. Upon arrival at the research center, study subjects were moved to a pre-op holding area where they were fitted with proper-size earbuds by a CTC on duty, the earbuds' signal quality was checked and a written consent was signed by study subjects prior to the procedure. Study subjects also wore IH earbuds for 3–5 min while at rest to gather baseline data. A dedicated room was used for a limited transthoracic echocardiogram (TTE) procedure performed by a designated sonographer. The left heart catheterization (LHC) procedure was performed in a surgery suite, with authorized personnel access only. The MindMics team participated in and operated the data collection remotely, by means of a teleconferencing system for connecting to a local computer at Scripps. While the order of the execution of the TTE and LHC procedures depended on departmental workflow for that day, the study protocol ensured that both the TTE and LHC were completed within a 2.5-h window. Throughout both procedures, study subjects continued to wear the MindMics earbuds to collect continuous data.

In the TTE part of the protocol, ~25–45 Echo images per study subject were collected simultaneously with the IH waveforms, with the Echo views corresponding to: AP 5C-CW Doppler AoV; AP 5C-PW Doppler LVOT; AP 3C-CW Doppler AoV; AP 3C-PW Doppler LVOT; and PW Doppler MV inflow. Each view was captured 2–5 times while the subject was at rest or performed the resonant breathing exercise and the Valsalva maneuver.

During the LHC procedure study subjects were at rest in a supine position. For each study subject, ~10–40 min of joint IH, ECG, and CC data were recorded, corresponding to ~500–2400 cardiac cycles. The data collection protocol included data with the tip of the catheter positioned in the aorta, but data from the left ventricle, radial/brachial or femoral arteries, and optionally left and right coronary arteries were recorded as well, depending on the type of the CC procedure. To increase variations in cardiac events, a minute of data from the aorta was recorded while the study subject performed breathing exercises. All data were recorded with the sampling rate of 1 kHz. In the analysis, the ECG, CC, and echocardiogram data are used to validate cardiac features in the IH waveforms, while the CC data from the aorta provide reference BP values for BP modeling.

The clinical equipment necessary for echocardiography and catheterization measurements was provided by Scripps Health. Medtronic, Terumo, and Boston Scientific coronary catheters were used to invasively measure blood pressure during the catheterization procedure. The catheterization room was equipped with a GE TRAM system, which is a multi-parameter

Table 1 | Overall study demographic

		CAD sample		CAD sample for analysis
Number of study subjects:		24		18
Age range (average):		39–85 (67)		49–85 (67)
Height range (average):		155–188 (173)		155–188 (173)
Weight range (average):		57–133 (89)		60–133 (89)
Gender (F/M):		6/18		5/13
Cardiovascular disease:	Obstructive CAD on procedure date		15	10
Comorbidities:	Hyperlipidemia		22	18
	Hypertension		16	11
	Diabetes		11	9
	Atrial fibrillation		4	3
	Heart failure		4	2
	Cerebrovascular accident		2	1
	Chronic kidney disease		1	1
	Valvular disease on echo		1	1

General clinical characteristics of subjects in the study. Numbers next to cardiovascular conditions correspond to the total number of study subjects diagnosed with those conditions.

module that simultaneously records multi-lead ECG signals and up to 4 channels with invasive blood pressure. The analogue output of the GE TRAM system and the MindMics IH earbuds were synchronized and recorded using a Data Acquisition System (DAQ) and sent to the computer over a wired USB connection and further to a MindMics cloud infrastructure using secured communication protocol MQTT, where the data was stored for future analysis. Overall there were 4 setups of devices available for this clinical study, each including a laptop computer to run the DAQ system, a set of MindMics IH earbuds, a hardware board hosting DAQ system and necessary cabling. The WiFi router was used to send the data from a laptop to the MindMics cloud. The echocardiogram data were recorded separately to a local Nucleus database in a form of high-resolution images, from where they were copied to a MindMics storage repository in the cloud; the time synchronization with MindMics signals was performed offline.

Consenting subjects participated in the study for about 3–5 h, including breaks between the procedures. This study involved only one visit to the Scripps clinic. There were no known risks to study subjects associated with wearing the MindMics earbuds during the procedure. The simultaneous data collection of signals from earbuds and catheter during a regularly scheduled catheterization procedure had a negligible effect on the outcome of the latter. Verbal communication between the study subject and the clinical coordinator was possible during the entire procedure, including times when the study subject wore earbuds. The protection of the privacy of study subjects was ensured by anonymizing the data by the Scripps CTC. All the study subjects' confidential information was removed from study reports before they were handed over to the MindMics team. The only available information included study subjects' sex, age, race, height, weight, classification of cardiovascular disease and comorbidities.

Study population
Table 1 shows an overall demographics for the CAD subjects in the study ($n = 24$), together with comorbidities. From the recruited subjects, 6 were discarded from the current analysis, because of issues with recording reference signals from the GE Tram unit (1 subject), an insufficient quality of ECG signals (2 subjects), or an insufficient earbud fit in study subjects' ears (3 subjects) that could not be resolved at the time of data collection

when the catheter head was in the aorta, due to limited access to the procedure area. The characteristics of the subjects selected for the analysis ($n = 18$) is as follows (also listed in Table 1): the age in the range between 49 and 85 (average 67) years, height between 155 and 188 (average of 173) cm, weight between 60 and 133 (average of 89) kg, 28% females. The fraction of females is comparable to the number observed in all cath procedures at Scripps (34%), which is similar for all Scripps hospitals. 10 subjects had obstructive CAD confirmed during the procedure.

Data preparation for analysis
Figure 9 shows a typical structure of the data collected during the CC procedure for one of the study subjects as an example. The top two plots present IH data collected with the left and the right earbuds, while the bottom plot displays blood pressure waveforms recorded with the catheter at different arterial and heart locations: the radial (yellow) and brachial (gold) arteries, the aorta (blue), the heart's left ventricle (red), and the coronary arteries (green area). The dark blue region corresponds to a minute of breathing exercises performed by the subject while the catheter head was in the aorta. Regions with very low pressure values correspond to the catheter's transitioning zones. The ECG signals are not shown in the figure. Only data with the catheter head in the aorta are selected for the blood pressure analysis, as described below.

For Wiggers diagrams shown in Figs. 1, 2, and Supplementary Figs. 1, 2, sets of 15 consecutive ECG, IH, and CC waveforms were arbitrarily selected from regions when the catheter head was in the aorta. For BP modeling a data processing pipeline was introduced to create the so-called databanks with simultaneous IH and CC waveforms of individual cardiac cycles. In this pipeline: (i) the IH data were corrected for instrumental effects using proprietary algorithms, (ii) the IH and CC signals were merged into events corresponding to individual cardiac cycles, with a cardiac cycle defined as the time between two consecutive QRS peaks of the ECG, (iii) a data quality assessment of the catheter and IH signals was performed by requiring a good cross-correlation score between individual waveforms and good-signal templates, to remove waveforms with motions artifacts or instrumental noise (Fig. 10 for a 30-sec period in an exemplary study subject) (iv) accepted cardiac cycles were written into csv files (databanks) for further analysis. Figure 11 shows the number of cardiac cycles with simultaneous IH and catheter waveforms for each of the CAD study subjects after all selections. In total, there are 2171 cardiac cycles (data points) for BP modeling and timing analysis. In this sample, 14 (11) subjects have good signals recorded in the left (right) earbud, while 7 subjects have good signals simultaneously recorded in both earbuds.

Comprehensive Wiggers diagrams and signal alignment
To evaluate the temporal relationships between cardiac events across multiple modalities, we generated a comprehensive set of Wiggers diagrams for study participants who underwent CC and had complete multimodal datasets comprising IH, 12-lead electrocardiography (ECG), echocardiography, and invasive aortic pressure recordings.

IH, aortic pressure, and ECG Lead II were recorded concurrently during CC at a sampling rate of 1 kHz. When available, peripheral pressure waveforms from the brachial, radial, and femoral arteries were also collected as the catheter advanced from the wrist or groin to the aorta. Although these peripheral traces were not acquired simultaneously with central signals, they serve to illustrate the progression of waveform morphology along the arterial tree. Doppler echocardiography of LVOT was typically obtained prior to catheterization and served as a reference for cycle timing.

To enable consistent temporal comparisons across modalities, cardiac cycles in both catheterization and IH signals were rescaled to match the inter-beat intervals (IBIs) extracted from the echocardiographic ECG trace. The signals were then aligned in time so that the QRS complexes in both echocardiogram and catheterization/IH ECGs were synchronized. Each Wiggers diagram panel includes, from top to bottom: LVOT Doppler flow, aortic pressure, IH waveform (corrected for instrument response), high-frequency IH (>20 Hz) revealing S1 and S2 sounds, and ECG Lead II. For
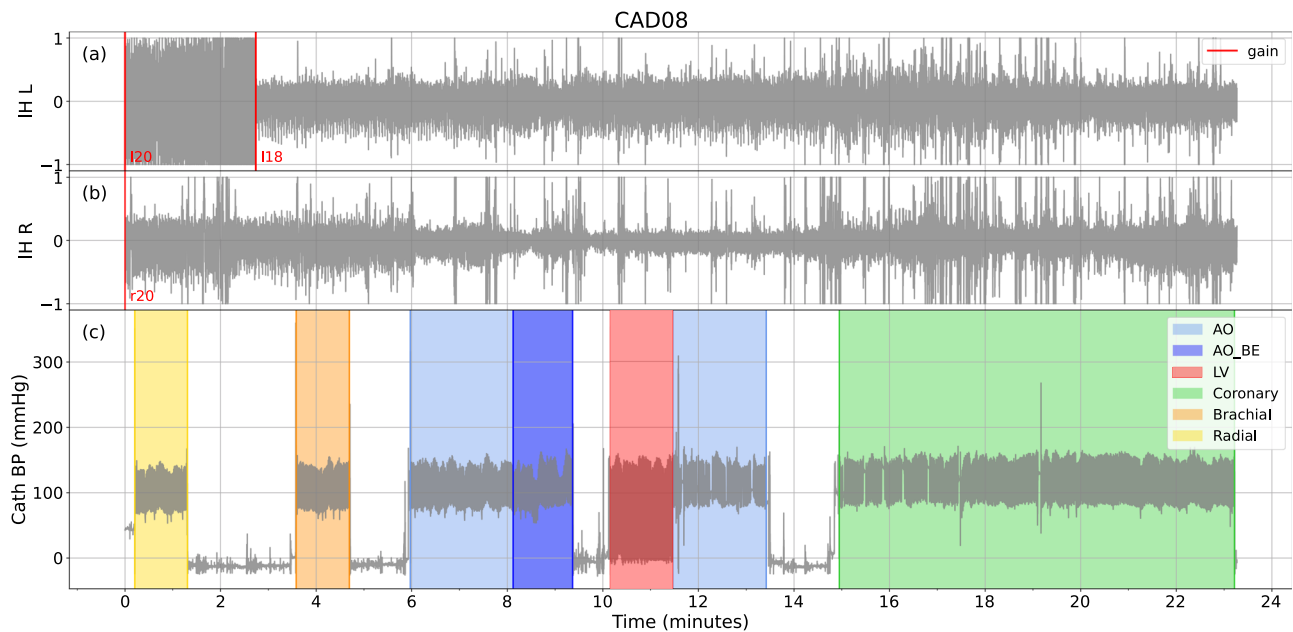
Fig. 9 | Exemplary data structure during the LHC procedure. Time series of the MindMics data from the **a** Left and **b** Right earbud, together with **c** the simultaneous catheter data for an exemplary study subject. Colors in the bottom plot indicate various catheter head locations (see text).
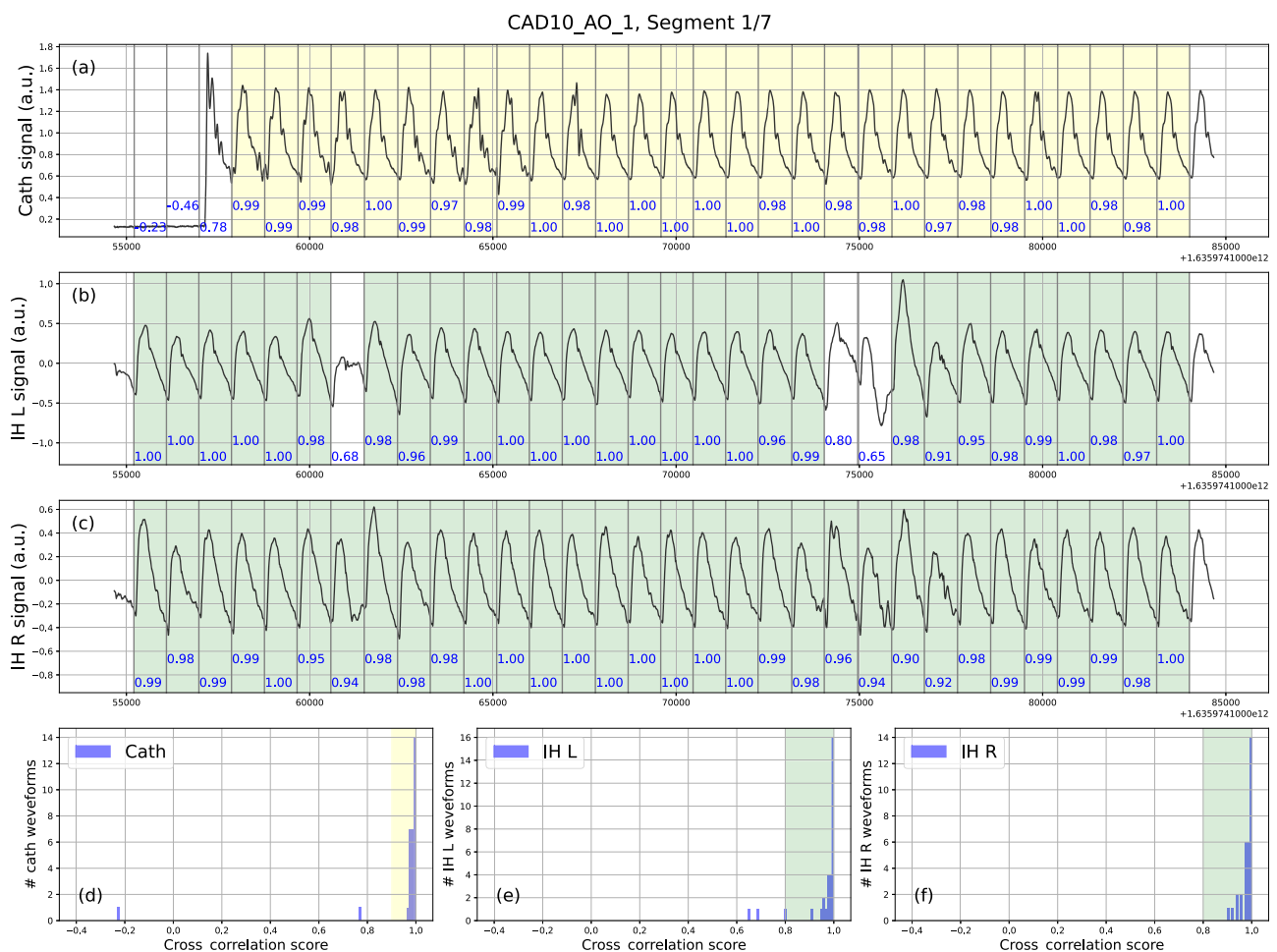

Fig. 10 | Data quality assessment. Data quality assessment of **a** simultaneous catheter and MindMics IH time series for **b** left and **c** right earbuds data shown for each cardiac cycle in an exemplary 30-s study subject's data. Cardiac cycles are defined by times between two consecutive QRS peaks of the ECG tracing (vertical lines). The distribution of signal quality, assessed using cross-correlation scores, is shown for **d** catheter waveforms, **e** IH signals from the left earbud, and **f** IH signals from the right earbud. Shaded regions indicate waveforms that passed the quality threshold.
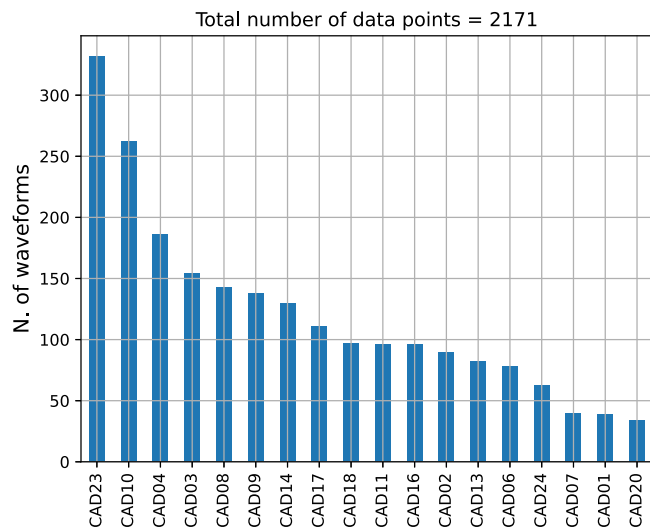
Fig. 11 | Number of cardiac cycles per CAD subject. Number of data points (cardiac cycles) for 18 study subjects who underwent cardiac catheterisation (CC) procedure for the evaluation of Coronary Artery Disease (CAD). Data points contain simultaneous in-ear IH and CC aortic pressure waveforms from individual heartbeats, defined by two consecutive QRS peaks of the ECG tracing. IH, CC, and ECG signals were recorded at a sampling rate of 1 kHz, and correspond to 30 s–6 min of data with the catheter head located in the aorta.

each subject, 15 consecutive cardiac cycles were typically stacked to compute average waveforms. In cases where fewer high-quality consecutive segments were available across all modalities—such as in CAD11 and CAD17—nine and eleven cycles, respectively, were used. Across all panels, variability around the averaged waveforms was primarily due to respiratory modulation of cardiac signals.

Figure 11 summarizes the number of analyzable cardiac cycles per study subject and serves as a guide to the grouping strategy. Group I includes subjects with more than 90 cycles, enabling the development of individualized blood pressure models (CAD 02, 03, 04, 08, 10, 11, 14, 16, 17, 18, and 23). Subjects CAD 06 and CAD 23 are presented in Figs. 1 and 2, respectively. Group II includes those with 15–89 analyzable cycles, who were included in one model for all analyses but not used for individual modeling (CAD 01, 06, 07, 09, 13, 20, and 24). Subjects CAD 05, 12, 15, and 19 were excluded due to incomplete IH or aortic pressure data; CAD 21 and 22 were excluded due to missing ECG. Wiggers diagrams for all included subjects are annotated with aortic valve opening (AVO) and closing (AVC) timings and shown in Supplementary Figs. 1 and 2.

Features for BP prediction

Many studies have explored feature extraction from hemodynamic waveforms for BP modeling using machine learning[25–27,52–59], particularly with peripheral PPG signals and reference SBP and DBP measurements from BP cuffs. Typically, a large set of potential features is generated based on various characteristic points of the waveform and their combinations. However, there is limited prior understanding of how these features correlate with BP dynamics. The challenge in determining feature-BP correlations arises because the BP signal from the cuff only provides the maximum and minimum values of the blood pressure waveform, which are also temporally separated.

The dataset used in this study includes full blood pressure waveforms recorded via a catheter positioned in the aorta, enabling a comparison of waveforms at different BP values to gain insights into how BP variations affect waveform shape. Figure 12 presents a comparison of normalized low- and high-BP waveforms, along with their first and second derivatives, from 4 exemplary study subjects. For each subject, the low- and high-BP waveforms were selected by minimizing and maximizing the product of SBP*DBP, respectively, as shown in the scatter plot.

Notable changes in the waveforms include the following: as BP increases, the waveforms become slightly narrower, with their maximum values delayed in time and the systolic portion shifted toward AVC. In the first derivative of the waveforms, the maximum at AVO remains largely unchanged with BP variations. However, the minimum at AVC becomes deeper, reflecting a more rapid decrease in pressure as the time approaches AVC at higher BP. It is also delayed. Similarly, changes in the second derivative occur mainly in the AVC region, with little variation observed in the AVO region.

Changes in heart rate (HR) appear to be a confounding factor when analyzing BP-induced changes in the waveform shape. However, HR variations primarily affect the diastolic phase of the cardiac cycle, causing its steeper exponential decline (Fig. 12a2, a4), while the duration of systole remains relatively unchanged.

The variations in waveform shape increase with BP changes. For examples shown in Fig. 12, the shape similarity expressed in terms of a cross correlation score decreases from 0.99 to 0.97 as the difference in SBP increases from 9 to 33 mmHg, respectively. When averaged over all subjects the score is 0.98 for the average SBP increase of 22 mmHg. We also calculated the cross correlation score for the difference in the waveform shape between the subjects at a fixed SBP. When averaged over all subjects pairs constructed from 9 (8) subjects that had measurement at SBP = 120 (130) ± 1 mmHg, the score is 0.95 (0.94). We conclude that in our sample, variations in the waveform shape due to BP changes are smaller than variations between subjects. This observation suggests that individualized BP prediction models, tailored to each subject, are likely to yield better performance than a single model applied across all subjects.

The waveform dynamics described above is used to create a list of features for BP prediction. These features, among others, include ratios of timings and normalized areas under the curve for selected parts of the cardiac cycle, the four leading moments of the systolic part, as well as amplitude ratios calculated at AVO and AVC times in the first and second derivatives of the waveforms. Other features in the list include waveform durations (interbeat intervals, IBIs) and the instantaneous heart rate, derived from these intervals. Finally, demographic variables such as sex, age, height, weight, body mass index (BMI), and body surface area (BSA) are incorporated when training a model for all subjects.

Machine learning model for BP prediction

Two approaches were used to predict SBP and DBP in the CC and IH data, based on features described in the previous section, extracted from individual cardiac-cycle waveforms after normalizing their amplitudes to the range of [0,1]: (i) we trained individual models for each of the study subjects, as well as (ii) one model for all the subjects. Features corresponding to demographic variables were used only in the latter case. Individual cardiac cycles were treated as a tabular rather than timeseries data, i.e. their time sequence was not used when training models. Reference SBP and DBP values were obtained from CC measurements, providing precision superior to that of traditional BP cuff devices (approx. 1 vs 5 mmHg, respectively).

For individual models, 12 subjects were used who had at least 1.5 min (≥ 90 cardiac cycles) of recorded data, to ensure a sufficient number of observations. Commonly used machine learning models from the scikit-learn library, such as SVM, KNN, LASSO and ElasticNet Regression, RandomForest and GradientBoosing ensemble-based models were trained to predict SBP and DBP. The results showed similar performance for the out-of-the-box models, slightly favoring the Gradient Boosting model (GBM) and LASSO Regression (LASSO) algorithms. In training and evaluating models for independent subjects, a 5-fold cross validation technique, with a 80/20% split for training/testing samples, was used. Table 2 shows model performance in terms of standard deviation between predicted and reference values of SBP and DBP for GBM and LASSO models, separately for CC and IH data, and for training and testing set. The numbers are evaluated after combining predictions from all 12 subjects. Given a limited sample size in this study, no full-scale hyperparameter tuning was performed for the GBM model, while the results for the LASSO model are shown with the regularization strength parameter changed from its default
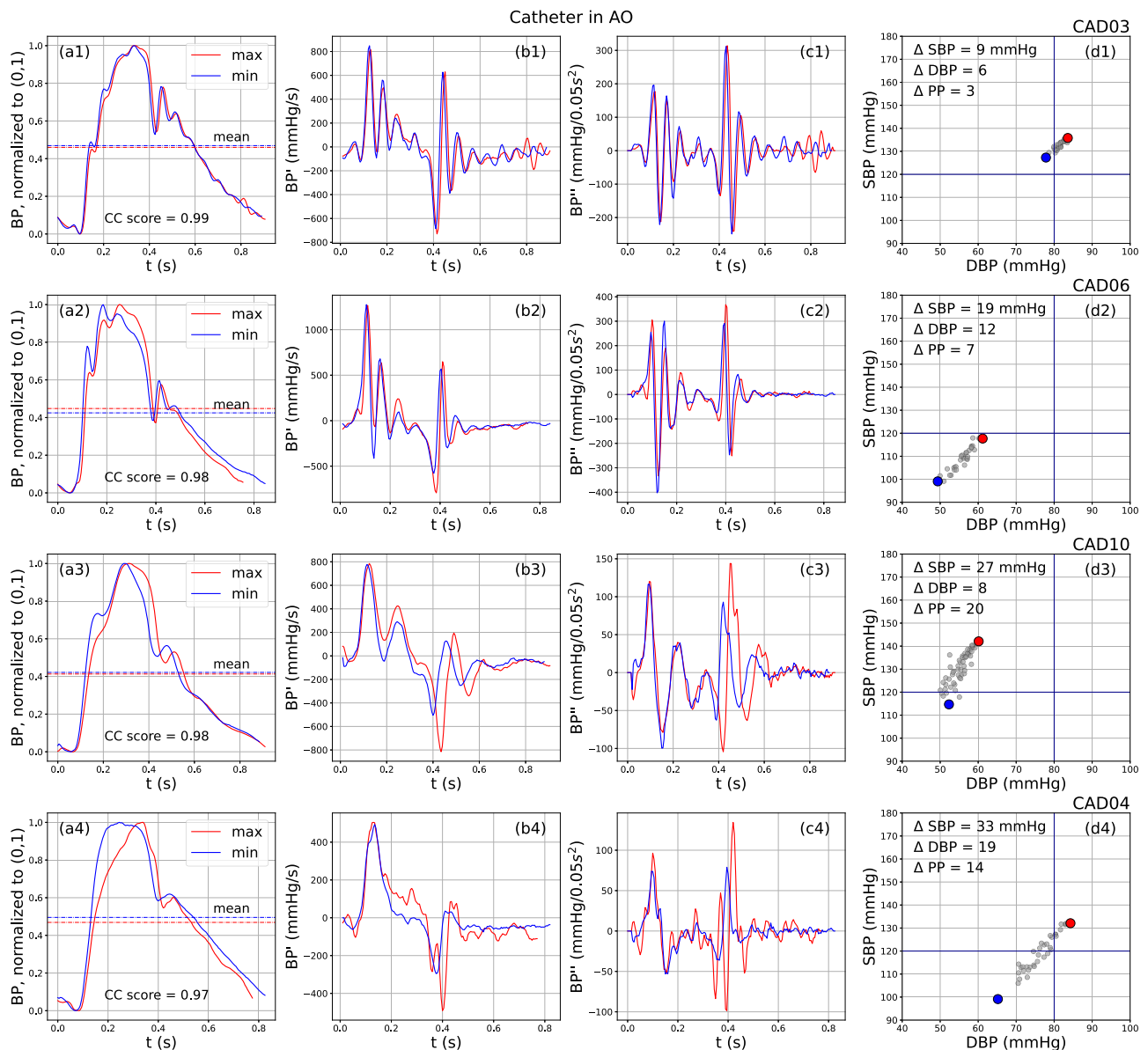
Fig. 12 | Comparison of CC waveforms at low/high BP. Shape comparison of **a** normalized cardiac catheterization (CC) waveforms and their **b** first and **c** second derivatives corresponding to a high (red) and low (blue) BP in 4 exemplary subjects (rows 1–4). For each subject, waveforms are selected by minimizing and maximizing the product of SBP*DBP, as depicted by colored dots in the scatter plots (**d**).

Differences in SBP, DBP, and PP = SBP-DBP between the two selected waveforms are indicated in the scatter plots as well. The duration of the cardiac cycle, also known as an interbeat interval (IBI), is inversely proportional to the subject's heart rate, i.e. a shorter (longer) IBI corresponds to a higher (lower) HR.

value $\alpha = 1$ to 0.1, as it gave a better performance in a quick parameter scan. The IH-predicted vs CC-measured BP values from the Gradient Boosting model for individual subjects are compiled on a common plot in Fig. 4, separately for the CC (top) and IH (bottom) data and for SBP (left) and DBP (right). The Bland-Altman plots with the relationship of agreement for predicted and reference values of SBP and DBP are shown in Fig. 5, using similar figure layout.

When averaged over all 12 subjects, the standard deviation of the difference between predicted and reference BP values were 4.1 and 2.4 mmHg for CC and 5.8 and 3.7 mmHg for MindMics data, for SBP and DBP, respectively. A very good agreement with the reference for the CC sample demonstrates that BP information is encoded in the waveform shape.

For completeness, we also trained one model for all subjects, although the dataset comprising 18 subjects is too small for the model to sufficiently capture physiological differences in the general population. In this approach, the so-called Leave-One-Out technique was used to separate

18 subjects into training and testing samples. Namely, 18 trainings were performed, with each subject contributing 17 times to the training set and one time to the testing set. As mentioned earlier, subjects' demographic variables were included in the list of input features. After aggregating the results of the GBM algorithm over all subjects, the standard deviation of the difference between predicted and reference values of SBP and DBP was 16.2 and 8.3 mmHg for CC data and 15.3 and 8.0 mmHg for IH data, respectively. Interestingly, when five data points from the test subjects were seeded to the training set, the model performance improved significantly, with the standard deviation of SBP and DBP prediction uncertainties reduced to 8.6 and 4.8 mmHg for CC data, and 9.8 and 5.7 mmHg for IH data, respectively. A discussion of these results is presented in the main text.

A preliminary feature importance analysis of the GBM and LASSO models revealed that although individual models differ in their set of most significant features, there is a common subgroup of features present in all subjects. These most frequent features include: the duration of the cardiac

Table 2 | Results of machine learning algorithms for predicting systolic and diastolic blood pressure

Model	Sample	Train set (80%) SBP/DBP [mmHg]	Test set (20%) SBP/DBP [mmHg]
GBM	CC	0.4/0.2 (1.00/1.00)	4.1/2.4 (0.96/0.98)
	IH	0.6/0.4 (1.00/1.00)	5.8/3.7 (0.92/0.95)
LASSO	CC	3.2/1.7 (0.97/0.99)	5.7/2.3 (0.92/0.98)
	IH	4.6/2.9 (0.95/0.97)	6.9/4.0 (0.88/0.95)

Standard deviation of the difference between predicted and reference values of systolic (SBP) and diastolic (DBP) blood pressure for Gradient Boosting model (GBM) and LASSO regression machine-learning algorithms using the CC and IH data. Results are shown separately for the training and test data sets. They were calculated by combining predictions of individual models from 12 study subjects selected as explained in the text. Numbers in brackets correspond to the Pearson correlation coefficients of predicted vs reference SBP/DBP distributions.

cycle (IBI) and its systole part (LVET), the area under the curve for the systole and the rapid ejection phase (from AVO to the waveform maximum) parts, moments of the systolic part of the waveform, the value of the normalized waveform at AVO and AVC, ratios of amplitudes of the first and second derivative at AVO and AVC, and the band power around AVO and AVC in various frequency bands from 0 to 50 Hz. For DBP, also the area under and diastolic part of the cardiac cycle and the slope of its exponential dependence are important for model prediction. A similar set of features appears to be important when training the multi-subject model, where, in addition, subjects' age, height, and BMI are frequently used. A larger set of cardiac cycles for training individual models and a larger set of subjects for the multi-subject model are needed to conclude this analysis.

Data availability

Datasets used for the analyses in this study are available from the corresponding author upon request.

Code availability

Models and code generated or used during the study are proprietary or confidential in nature and may only be provided with restriction.

References

1. Wierzejska, E. et al. A global perspective on the costs of hypertension: a systematic review. *Arch. Med. Sci.* **16**, 1078–1091 (2020).
2. Daly, J. et al. Barriers to Participation in and Adherence to Cardiac Rehabilitation Programs: A Critical Literature Review. *Prog. Cardiovasc. Nurs.* **17**, 8–17 (2002).
3. Zaree, A. et al. Cardiac rehabilitation in the modern era: optimizing recovery and reducing recurrence. *Cureus* **15**, e46006 (2023).
4. Kirkland, E. B. et al. Trends in healthcare expenditures among US adults with hypertension: national estimates, 2003-2014. *J. Am. Heart Assoc.* **7**, e008731 (2018).
5. Bhandari, B., Narasimhan, P., Vaidya, A., Subedi, M. & Jayasuriya, R. Barriers and facilitators for treatment and control of high blood pressure among hypertensive patients in Kathmandu, Nepal: a qualitative study informed by COM-B model of behavior change. *BMC Public Health* **21**, 1524 (2021).
6. Dzau, V. J. & Hodgkinson, C. P. Precision hypertension. *Hypertension* **81**, 702–708 (2024).
7. Zhou, B. et al. Worldwide trends in hypertension prevalence and progress in treatment and control from 1990 to 2019: a pooled analysis of 1201 population-representative studies with 104 million participants. *Lancet* **398**, 957–980 (2021).
8. Hughes, A., Shandhi, M. M. H., Master, H., Dunn, J. & Brittain, E. Wearable devices in cardiovascular medicine. *Circ. Res.* **132**, 652–670 (2023).
9. Hare, A. J., Chokshi, N. & Adusumalli, S. Novel digital technologies for blood pressure monitoring and hypertension management. *Curr. Cardiovasc. Risk Rep.* **15**, 11 (2021).
10. Bhavnani, S. P., Narula, J. & Sengupta, P. P. Mobile technology and the digitization of healthcare. *Eur. Heart J.* **37**, 1428–1438 (2016).
11. Bard, D. M., Joseph, J. I. & van Helmond, N. Cuff-less methods for blood pressure telemonitoring. *Front. Cardiovasc. Med.* **6**, 40 (2019).
12. Gilliam, F. R. et al. In-ear infrasonic hemodynography with a digital health device for cardiovascular monitoring using the human audiome. *npj Digit. Med.* **5**, 189 (2022).
13. Gilliam, F. R. et al. B-AB24-01 MindMics: in-ear infrasonic hemodynography for cardiac arrhythmia assessment beyond ECG. *Heart Rhythm.* **18**, S46 (2021).
14. Wheeler, C. M. et al. Abstract 11669: "hearing the heart" - validation of a novel digital health earbud technology to measure cardiac time intervals through infrasonic hemodynography. *Circulation* **144**, (2021).
15. Shen, C. P. et al. A novel earbud detects aortic stenosis murmur before and after transcatheter aortic valve replacement. *JACC: Case Rep.* **28**, 102089 (2023).
16. Waldman, C. E. et al. Abstract 13654: can a novel earbud technology detect severe aortic stenosis? Modernizing the Wiggers diagram through infrasonic hemodynography synchronized with echocardiography and cardiac catheterization. *Circulation* **144**, (2021).
17. Klabunde, R. E. *Cardiovascular physiology concepts*, 3rd ed. (Lippincott Williams & Wilkins, 2021).
18. Teo, S. G., Yang, H., Chai, P. & Yeo, T. C. Impact of left ventricular diastolic dysfunction on left atrial volume and function: a volumetric analysis. *Eur. J. Echocardiogr.* **11**, 38–43 (2010).
19. Gill, H. & Hoffmann, A. The timing of onset of mechanical systole and diastole in reference to the QRS-T complex: a study to determine performance criteria for a non-invasive diastolic timed vibration massage system in treatment of potentially unstable cardiac disorders. *Cardiovasc. Eng.* **10**, 235–245 (2010).
20. Aziz, F., Tk, L. A., Enweluzo, C., Dutta, S. & Zaeem, M. Diastolic heart failure: a concise review. *J. Clin. Med. Res.* **5**, 327–334 (2013).
21. Attenhofer Jost, C. H. et al. Echocardiography in the evaluation of systolic murmurs of unknown cause. *Am. J. Med.* **108**, 614–620 (2000).
22. Vasan, R. S., Benjamin, E. J. & Levy, D. Congestive heart failure with normal left ventricular systolic function. Clinical approaches to the diagnosis and treatment of diastolic heart failure. *Arch. Intern. Med.* **156**, 146–157 (1996).
23. Westerhof, N., Lankhaar, J.-W. & Westerhof, B. E. The arterial Windkessel. *Med. Biol. Eng. Comput* **47**, 131–141 (2009).
24. Lombard, J. T. & Selzer, A. Valvular aortic stenosis: a clinical and hemodynamic profile of patients. *Ann. Intern Med.* **106**, 292–298 (1987).
25. Mieloszyk, R. et al. A comparison of wearable tonometry, photoplethysmography, and electrocardiography for cuffless measurement of blood pressure in an ambulatory setting. *IEEE J. Biomed. Health Inform.* **26**, 2864–2875 (2022).
26. Mukkamala, R., Stergiou, G. S. & Avolio, A. P. Cuffless blood pressure measurement. *Ann. Rev. Biomed. Eng.* **24**, 203–230 (2022).
27. Mukkamala, R. et al. Toward ubiquitous blood pressure monitoring via pulse transit time: theory and practice. *IEEE Trans. Biomed. Eng.* **62**, 1879–1901 (2015).
28. Colvonen, P. J. Response to: investigating sources of inaccuracy in wearable optical heart rate sensors. *npj Digit. Med.* **4**, 38 (2021).
29. Schutte, A. E., Kollias, A. & Stergiou, G. S. Blood pressure and its variability: classic and novel measurement techniques. *Nat. Rev. Cardiol.* **19**, 643–654 (2022).
30. Wiggers, C. *Circulation in health and disease* (Lea & Febiger, 1915).
31. Gyöngy, M. & Kollár, S. Variation of ultrasound image lateral spectrum with assumed speed of sound and true scatterer density. *Ultrasonics* **56**, 370–380 (2015).

32. Blacher, J., Asmar, R., Djane, S., London, G. M. & Safar, M. E. Aortic pulse wave velocity as a marker of cardiovascular risk in hypertensive patients. *Hypertension* **33**, 1111–1117 (1999).

33. Pilz, N. et al. Pulse wave velocity: methodology, clinical applications, and interplay with heart rate variability. *Rev. Cardiovasc. Med.* **25**, 266 (2024).

34. Sorensen, G. L., Jensen, J. B., Udesen, J., Holfort, I. K. & Jensen, J. A. Pulse wave velocity in the carotid artery. In *2008 IEEE Ultrasonics Symposium*, 1386–1389 https://doi.org/10.1109/ULTSYM.2008.0336 (2008).

35. Alecu, C. et al. Reference values of aortic pulse wave velocity in the elderly. *J. Hypertens.* **26**, 2207–2212 (2008).

36. Ungerleider, R. M., Nelson-McMillan, N., Cooper, D. S., Meliones, J. N. & Jacobs, J. *Critical heart disease in infants and children*, 3rd ed. (Elsevier, 2019).

37. Luis, S. A., Chan, J. & Pellikka, P. A. Echocardiographic assessment of left ventricular systolic function: an overview of contemporary techniques, including speckle-tracking echocardiography. *Mayo Clin. Proc.* **94**, 125–138 (2019).

38. Bonow, R. O. *Valvular heart disease: a companion to braunwald's heart disease*, 5th ed. (Elsevier, 2020).

39. Little, W. C. & Downes, T. R. Clinical evaluation of left ventricular diastolic performance. *Prog. Cardiovasc. Dis.* **32**, 273–290 (1990).

40. Feher, J. *Quantitative human physiology*, 2nd ed. (Academic Press, 2017).

41. Alhakak, A. S. et al. The cardiac isovolumetric contraction time is an independent predictor of incident heart failure in the general population. *Int. J. Cardiol.* **312**, 81–86 (2020).

42. Sinanis, T. et al. Isovolumetric contraction as a marker of ventricular performance in patients with afterload mismatch. *Diagnostics* **13**, 1366 (2023).

43. Allen, J. & Murray, A. Age-related changes in peripheral pulse timing characteristics at the ears, fingers and toes. *J. Hum. Hypertens.* **16**, 711–717 (2002).

44. Martin, A. & Voix, J. In-ear audio wearable: measurement of heart and breathing rates for health and safety monitoring. *IEEE Trans. Biomed. Eng.* **65**, 1256–1263 (2018).

45. Butkow, K.-J., Dang, T., Ferlini, A., Ma, D. & Mascolo, C. hEARt: motion-resilient heart rate monitoring with in-ear microphones. In *2023 IEEE International Conference on Pervasive Computing and Communications (PerCom)* 200–209 https://doi.org/10.1109/PERCOM56429.2023.10099317 (2023).

46. Chen, T. et al. Exploring the feasibility of remote cardiac auscultation using earphones. In *Proceedings of the 30th Annual International Conference on Mobile Computing and Networking* 357–372 https://doi.org/10.1145/3636534.3649366 (2024).

47. Goverdovsky, V., Looney, D., Kidmose, P., Papavassiliou, C. & Mandic, D. P. Co-located multimodal sensing: a next generation solution for wearable health. *IEEE Sens. J.* **15**, 138–145 (2015).

48. Fan, X., Pearl, D., Howard, R., Shangguan, L. & Thormundsson, T. APG: audioplethysmography for cardiac monitoring in hearables. In *Proceedings of the 29th Annual International Conference on Mobile Computing and Networking* 1–15, https://doi.org/10.1145/3570361.3613281 (2023).

49. Gaardbaek, B. & Kidmose, P. On the origin of cardiovascular sounds recorded from the ear. *IEEE Trans. Biomed. Eng.* **72**, 210–216 (2025).

50. Christofferson, K., Bhalla, S., Cafazzo, J. & Mariakakis, A. On the production and measurement of cardiac sounds in the ear canal. In *Companion of the 2024 on ACM International Joint Conference on Pervasive and Ubiquitous Computing* 685–690, https://doi.org/10.1145/3675094.3680526 (2024).

51. Barnacka, A. et al. System and method for leak correction and normalization of in-ear pressure measurement for hemodynamic monitoring, US patent 20210401311 (2021).

52. Chowdhury, M. H. et al. Estimating blood pressure from the photoplethysmogram signal and demographic features using machine learning techniques. *Sensors* **20**, 3127 (2020).

53. Alghamdi, A. S., Polat, K., Alghoson, A., Alshdadi, A. A. & Abd El-Latif, A. A. Gaussian process regression (GPR) based non-invasive continuous blood pressure prediction method from cuff oscillometric signals. *Appl. Acoust.* **164**, 107256 (2020).

54. Natarajan, K. et al. Photoplethysmography fast upstroke time intervals can be useful features for cuff-less measurement of blood pressure changes in humans. *IEEE Trans. Biomed. Eng.* **69**, 53–62 (2022).

55. Truong, H., Montanari, A. & Kawsar, F. Non-invasive blood pressure monitoring with multi-modal in-ear sensing. In *IEEE International Conference on Acoustics, Speech and Signal Processing (ICASSP)* 6–10 https://doi.org/10.1109/ICASSP43922.2022.9747661 (IEEE, 2022).

56. Mukkamala, R. et al. The Microsoft Research Aurora project: important findings on cuffless blood pressure measurement. *Hypertension* **80**, 534–540 (2023).

57. Nour, M., Polat, K., Şentürk, Ü & Arıcan, M. A novel cuffless blood pressure prediction: uncovering new features and new hybrid ML models. *Diagnostics* **13**, 1278 (2023).

58. Liu, Z.-D. et al. Cuffless blood pressure measurement using smartwatches: a large-scale validation study. *IEEE J. Biomed. Health Inform.* **27**, 4216–4227 (2023).

59. Kasbekar, R. S., Ji, S., Clancy, E. A. & Goel, A. Optimizing the input feature sets and machine learning algorithms for reliable and accurate estimation of continuous, cuffless blood pressure. *Sci. Rep.* **13**, 7750 (2023).

Acknowledgements

Author contributions

All authors contributed to the drafting of the manuscript and have reviewed and approved the submitted version. A.B. conceived the idea of IH and led the project with support from R.C. A.B., S.R., J.P., and M.R. collaboratively designed the study. Data collection for the study subjects was carried out by R.C., J.P., C.W., C.D., A.W., and H.E. J.P. was responsible for building and maintaining the hardware and devices used for data collection. R.C. led the data analysis and algorithm development, with contributions from J.P., J.G., M.R., and feedback from A.B. C.W., S.R., C.S., J.A., and M.R. reviewed the manuscript and provided valuable feedback.

Competing interests

The Authors declare no Competing Non-Financial Interests but the following Competing Financial Interests: authors affiliated with MindMics, Inc. received salary or equity or both, while authors affiliated with Scripps Health were contracted to perform data collection; M.R. and J.A. are advisors to MindMics, Inc. and received the company's stock options. Two patent applications most relevant to this study have been filed by MindMics, Inc., with A.B. and other MindMics affiliates including J.P. and M.R. listed as inventors. The first, US Patent No. 11,844,618 B2, titled "System and Method for Cardiovascular Monitoring and Reporting," has been granted and covers the core methodology of using in-ear infrasonic signals for non-invasive monitoring of cardiovascular parameters, including blood pressure—central to the approach validated in this feasibility study. The second, US Patent Application No. US 20210401311 A1, titled "System and Method for Leak Correction and Normalization of In-Ear Pressure Measurement for Hemodynamic Monitoring," was filed on December 20, 2021, and remains pending. It addresses signal correction techniques for mitigating acoustic leakage in the ear canal, which are critical to ensuring accurate biosignal acquisition and interpretation in the

Article

study's signal processing pipeline. Both filings support the underlying technology evaluated in the present manuscript.

Additional information